Top Organomet Chem (2021) 68: 263–320
https://doi.org/10.1007/3418_2020_63

Published online: 29 December 2020

Hydrogenation Reactions Catalyzed by PNP-Type Complexes Featuring a $HN(CH_2CH_2PR_2)_2$ Ligand

Dewmi A. Ekanayake and Hairong Guan

Contents

Abstract This chapter first provides a brief background of how hydrogenation mechanisms have evolved over the years leading to the blossom of catalytic systems with metal-ligand cooperativity. The main body of the chapter focuses specifically on complexes supported by ligands of the type $HN(CH_2CH_2PR_2)_2$. The discussion of hydrogenation systems is organized based on the central metals including Ru, Fe, Os, Rh, Co, Ir, Ni, Pd, Mo, W, Mn, and Re (in that particular order). Substrates involved in these hydrogenation reactions include olefins, aldehydes, ketones, esters,

D. A. Ekanayake and H. Guan (✉)
Department of Chemistry, University of Cincinnati, Cincinnati, OH, USA
e-mail: hairong.guan@uc.edu

amides, epoxides, nitriles, imines, *N*-heterocycles, CO_2 (to formate or methanol), silyl formates, CO (to ethylene glycol or methanol), and cyclic carbonates. When appropriate, the presence or the lack of metal-ligand cooperativity in these catalytic systems is highlighted.

Keywords CO_2 reduction · Hydride · Hydrogenation · Metal-ligand cooperativity · Pincer complexes

1 Introduction

The development of well-defined transition metal-based catalysts for hydrogenation reactions has been an active research area for almost half a century [1–4]. Early efforts were focused on catalytic hydrogenation of C=C (or C ≡ C) bonds. The generalized and simplified reaction mechanism involves oxidative addition of H_2 and coordination of the C=C bond to the metal (Scheme 1, Cycle A). These two steps can occur in either order, as exemplified by Wilkinson's $RhCl(PPh_3)_3$ catalyst for hydrogenating olefins (H_2 first) [5] and Halpern's $[(CHIRAPHOS)Rh(solvent)_2]^+$ catalyst for hydrogenating α-aminoacrylic acid derivatives (C=C bond first) [6]. In any case, subsequent C=C insertion into the metal-hydrogen bond followed by reductive elimination of the hydrogenation product completes the catalytic cycle. Hydrogenation reactions can also be catalyzed by a monohydride such as $RuHCl(PPh_3)_3$, whose mechanism (Scheme 1, Cycle B) usually features hydrogenolysis of a metal alkyl intermediate generated from C=C insertion [7].

Catalytic hydrogenation of C=O bonds in aldehydes and ketones, especially those without a neighboring heteroatom to assist carbonyl coordination, was

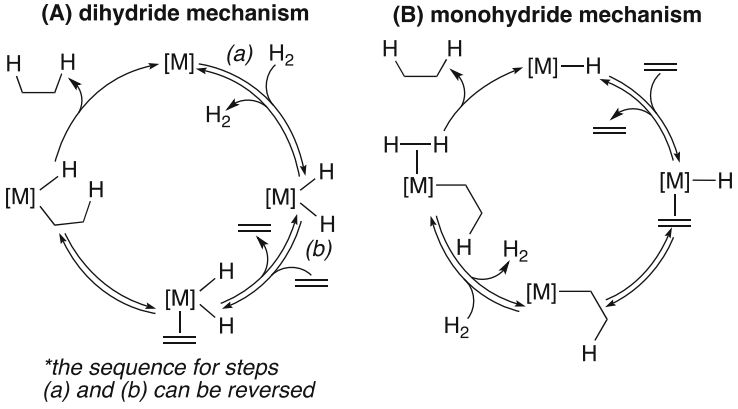

Scheme 1 Generalized mechanisms for catalytic hydrogenation of C=C bonds

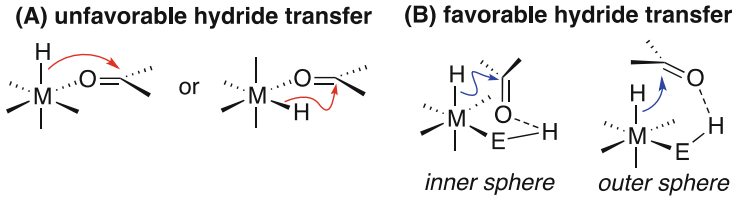

Scheme 2 Hydride transfer pathways

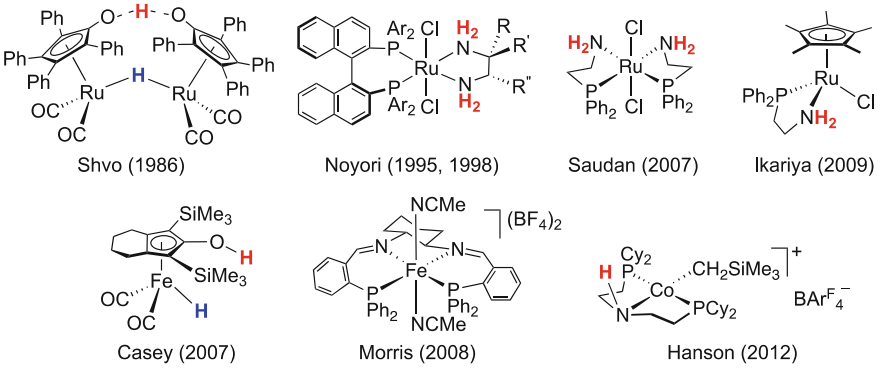

Fig. 1 Representative hydrogenation (pre)catalysts (acidic and hydridic hydrogens are highlighted)

developed much later. Noyori attributed the difficulty to the preferred coordination mode adopted by the carbonyl group [8]. Unlike olefinic substrates, simple aldehydes and ketones often coordinate to metals via the oxygen lone pair instead of the π system [9], which places the carbonyl carbon far away from the hydride to be delivered (Scheme 2, Pathway A). To overcome this issue, Noyori proposed to design catalysts with an acidic hydrogen strategically situated in the ligand scaffold so that it can protonate or form a hydrogen bond with the carbonyl oxygen, forcing an η^2-coordination mode for the C=O bond (Scheme 2, Pathway B). Alternatively, in an outer-sphere mechanism, the hydrogen-bonded substrate is brought to the close proximity of the hydride ligand for the desired hydride transfer.

The concept of metal-ligand cooperativity described above has significantly advanced the field of homogeneous hydrogenation. In particular, the E–H···O interaction illustrated in Pathway B (Scheme 2) potentially activates the carbonyl group and deemphasizes the role that the metal needs to play. It is therefore not a coincidence that the past decade has witnessed a rapid development of hydrogenation catalysts targeting more challenging substrates such as esters [10, 11] and amides [12, 13] and/or focusing on first-row transition metals including iron [14, 15] and cobalt [16]. Some of these hydrogenation (pre)catalysts as well as the earlier ones developed by Shvo [17] and Noyori [18, 19] are highlighted in Fig. 1.

The vast majority of metal-ligand bifunctional catalysts used for hydrogenation reactions contain at least one NH or NH_2 donor, which can be preinstalled prior to

Scheme 3 Catalyst activation strategies

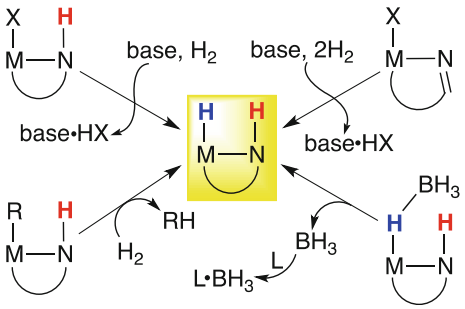

Scheme 4 Simplified catalytic cycle and transition state

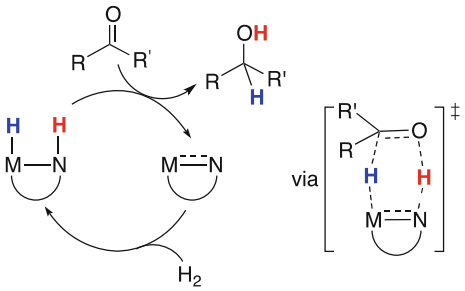

complexation or formed under hydrogenation conditions (e.g., hydrogenation of ligand C=N bonds) [20]. Although occasionally it is possible to synthesize the H–M–N–H-type complex first [21], most catalytic systems generate this active species in situ from various precatalysts (Scheme 3). Effective catalyst activation strategies include (1) removal of HX (X = Cl, Br, etc.) by a strong base followed by H_2 activation [11], (2) hydrogenolysis of a metal alkyl species [16], and (3) unmasking the hydride from the corresponding borohydride complex with heating or in the presence of a BH_3 scavenger [22].

It had been hypothesized that hydrogenation of C=O bonds catalyzed by H–M–N–H-type complexes would proceed via a concerted H^+/H^- transfer to the substrate followed by heterolytic cleavage of H_2 by the resulting amido species (Scheme 4) [23]. The lost catalytic activity in replacing NH with an NMe donor group is usually an indication of metal-ligand bifunctional catalysis [24]. However, DFT calculations [25] and kinetic studies [26] suggest that the mechanism is more nuanced than initially thought. For example, the delivery of H^+/H^- to the substrate can be asynchronous, and the alcohol product can serve as a proton shuttle for H_2 activation. Furthermore, the metal-bound NH functionality may merely play the role of stabilizing the transition states (through hydrogen bonding interactions) rather than participating in H^+ transfer [27]. There are also a number of hydrogenation systems in which alkylation of the NH functionality still results in an active catalyst [28]. Nevertheless, the success of employing H–M–N–H-type complexes as hydrogenation catalysts is evident and likely to provide the momentum to develop new catalysts featuring this particular structural motif.

This chapter focuses specifically on complexes supported by ligands of the type $HN(CH_2CH_2PR_2)_2$ ($^{R}PN^{H}P$ for short), which are arguably among the most extensively studied hydrogenation catalysts in recent years [29]. Our discussion starts with how these ligands are made and how they are used to prepare the PNP-type complexes. The subsequent overview of hydrogenation catalysis is organized based on the metals, starting from the more popular group 8 elements, transitioning to those in groups 9 and 10, and concluding with mid-transition metals.

2 Ligand Synthesis and Coordination Modes

The more frequently used $^{R}PN^{H}P$ ligands (R = ^{i}Pr, Cy, Ad or 1-adamantyl, ^{t}Bu) are commercially available in the neat form or as a THF solution, whereas $^{Ph}PN^{H}P$ is typically sold as a hydrochloride salt. If needed, they can be synthesized from $[H_2N(CH_2CH_2Cl)_2]Cl$ in one or few steps, depending on the properties of the phosphorus substituents (Scheme 5). Synthesis of $^{Ph}PN^{H}P$ or other aryl-substituted ligands is readily accomplished by refluxing $[H_2N(CH_2CH_2Cl)_2]Cl$ with the corresponding secondary phosphine in the presence of KO^{t}Bu [30–32]. Introducing alkyl groups as the phosphorus substituents requires nitrogen protection with a trimethylsilyl group prior to the addition of a lithium dialkylphosphide for the nucleophilic substitution reaction [33–36]. Hydrolysis of the resulting $Me_3SiN(CH_2CH_2PR_2)_2$ restores the NH moiety, which is occasionally performed in the presence of $^{n}Bu_4NF$ [37] or a 2 M solution of H_2SO_4 [35] to promote the N–Si bond cleavage. For purification purpose, the crude products are sometimes protonated by a dilute aqueous HCl solution to yield the hydrochloride salts as precipitates [30, 32, 34], and the free $^{R}PN^{H}P$ ligands are released following the treatment with NaOH or KOH.

Chiral $^{R}PN^{H}P$ ligands are also known in the literature (Scheme 6). Chirality has been introduced through the use of a phosphide derived from (2*S*,5*S*)-2,5-dimethyl-1-phenylphospholane [38] or an enantiomerically pure secondary phosphine-borane $H_3B{\bullet}PH(R)Me$ (R = ^{t}Bu, Cy) [39]. In the latter case, lithiation of $H_3B{\bullet}PH(R)Me$ and the subsequent nucleophilic substitution reaction are stereospecific, resulting in stereo-retention at the phosphorus center. In contrast, the in situ generated Li

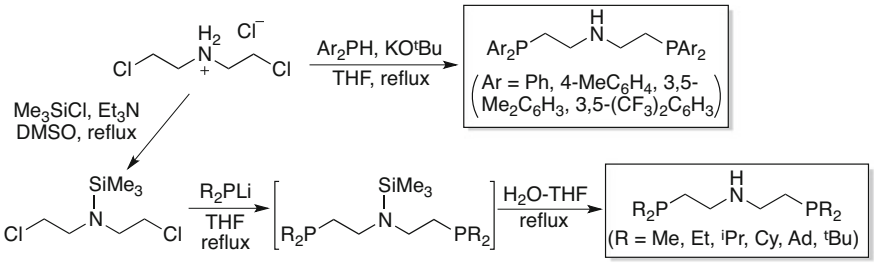

Scheme 5 Synthesis of achiral $^{R}PN^{H}P$ ligands

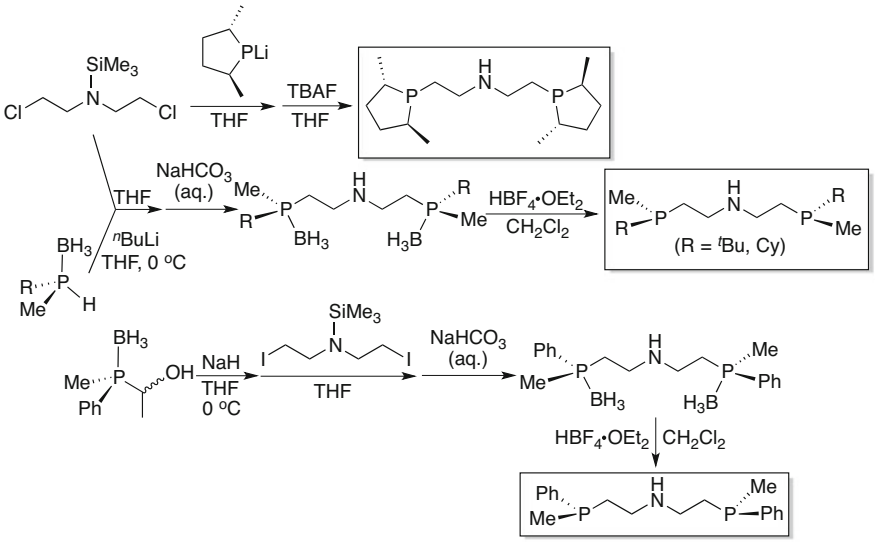

Scheme 6 Synthesis of chiral $^{R}PN^{H}P$ ligands

$[H_3BPPhMe]$ is configurationally unstable. Synthesis of the corresponding chiral $^{R}PN^{H}P$ ligand thus relies on the use of (S_P)-(1-hydroxyethyl) methylphenylphosphine-borane as a masked secondary phosphine-borane and $Me_3SiN(CH_2CH_2I)_2$ as a more reactive electrophile to minimize the chance for racemization [39]. The borane-protected $^{R}PN^{H}P$ ligands can be handled in air, and the removal of BH_3 by $HBF_4{\bullet}OEt_2$ is often carried out right before complexation.

The $^{R}PN^{H}P$ ligands or their deprotonated form $[N(CH_2CH_2PR_2)_2]^-$ (abbreviated here as ^{R}PNP) have been employed to make complexes of virtually every metal in groups 4–11 [40]. The coordination chemistry of these ligands is rich, exhibiting a variety of modes including κ^1-N [41], κ^2-P,N [42], κ^2-P,P [43], κ^3-P,N,P, and μ_2-P,P [44]. As far as hydrogenation catalysts are concerned, the κ^3-P,N,P coordination mode is most relevant, because it not only provides an entry to the H–M–N–H species but also stabilizes the metal complexes. As tridentate ligands, $^{R}PN^{H}P$ or ^{R}PNP can adopt a meridional or facial configuration, depending on the phosphorus substituents, metals, and ancillary ligands. To illustrate this point, Fig. 2 summarizes the solid-state structures of $(^{R}PN^{H}P)FeX_2$ [45–47] and $(^{R}PN^{H}P)CoX_2$ [48–53] known to date. The solution structures of $(^{iPr}PN^{H}P)FeCl_2$ probed by Mössbauer and magnetic circular dichroism spectroscopy also suggest that these PNP-type ligands are flexible in binding with metals [45].

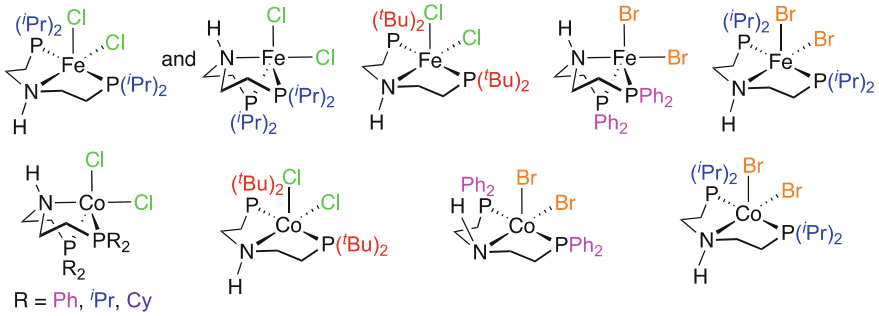

Fig. 2 Solid-state structures of (^{R}PN^{H}P)MX$_2$ studied by X-ray crystallography

3 Group 8 Metal Systems

3.1 Ruthenium Catalysts

3.1.1 Synthesis of (Pre)catalysts

Synthetic routes to hydrogenation (pre)catalysts involving ruthenium-based PNP-type complexes are summarized in Scheme 7. Complex (^{Ph}PN^{H}P)RuHCl (CO) was first developed by Takasago International Corporation with a trademark name of **Ru-MACHO** [32, 54]. It was originally isolated as a mixture of *syn* and *anti* (referring to the relative configuration of N*H* and Ru*H*) isomers from the reaction of ^{Ph}PN^{H}P with RuHCl(CO)(PPh$_3$)$_3$ performed in refluxing toluene, although minor modifications to the procedures could lead to the *anti* isomer only [55, 56]. The presence of two isomers is deemed to be unimportant for the hydrogenation reactions because catalyst activation by a base (Scheme 3) removes the NH hydrogen. The synthetic approach has been successfully extended to other ^{R}PN^{H}P ligands [55–57] including the one bearing chiral phospholane rings [58]. Substitution of the chloride in **Ru-MACHO**, **^{iPr}RuHCl**, and **^{Cy}RuHCl** for BH_4^- and H^- has been accomplished through the addition of $NaBH_4$ [32, 56, 59] and $NaBEt_3H$ [56, 60], respectively. The latter reaction with the sterically crowded **^{tBu}RuHCl**, however, produces a five-coordinate ruthenium hydride, likely due to a facile H_2 elimination from the initial product **^{tBu}RuH$_2$** [56]. The phenyl analog **^{Ph}RuH$_2$** synthesized from the $NaBEt_3H$ method has a low purity because of rapid decomposition [56]. It can alternatively be synthesized from **Ru-MACHO** and KO^{t}Bu (or KN(SiMe$_3$)$_2$) under H_2, though contaminated with ~5% of **Ru-MACHO** [21].

Other ruthenium precursors have been used to prepare PNP-type hydrogenation (pre)catalysts. The reaction of Ru(COD)(2-methylallyl)$_2$ with ^{tBu}PN^{H}P under 5 bar of H_2 produces a mixture of **^{tBu}RuH$_2$(H$_2$)** and **^{tBu}RuH(H$_2$)** (Scheme 7, Method B) [61]. Pure **^{tBu}RuH(H$_2$)** can be obtained by stirring the mixture under argon, and its reaction with a primary alcohol also affords **^{tBu}RuH** as a result of alcohol dehydrogenation and decarbonylation [62]. Using (*p*-cymene)RuCl$_2$(NHC) (NHC = 1,3-dimethylimidazol-2-ylidene) as the ruthenium source provides an opportunity to

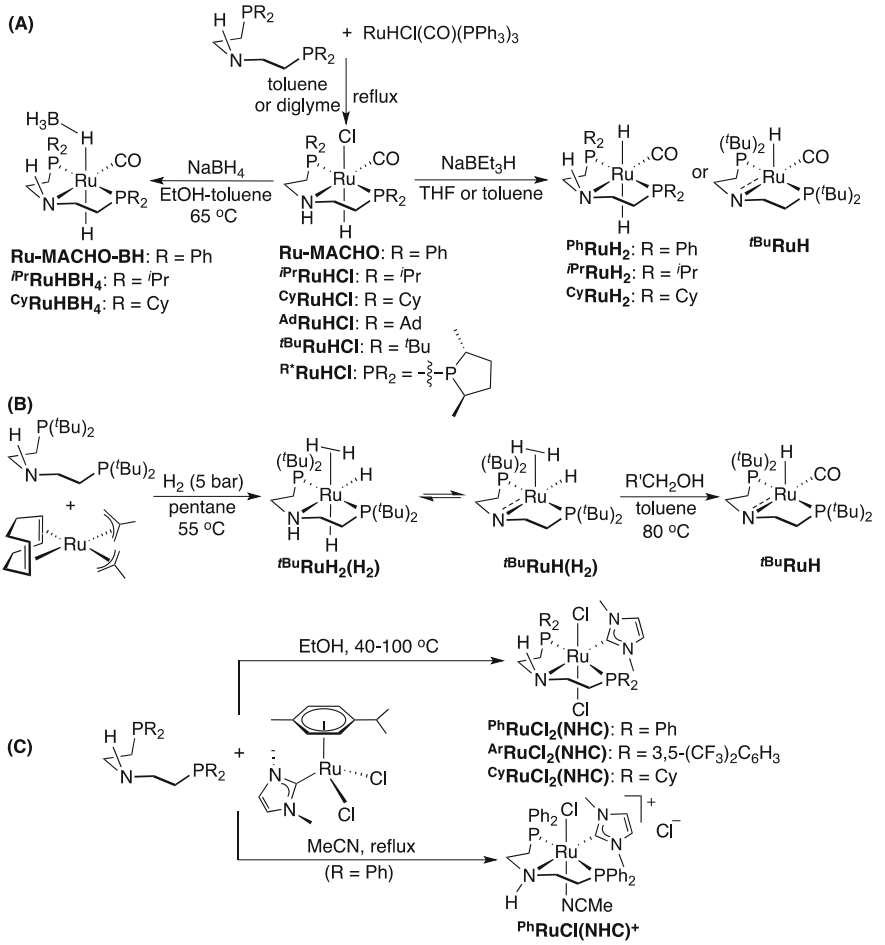

Scheme 7 Synthetic routes to ruthenium-based hydrogenation (pre)catalysts

incorporate an *N*-heterocyclic carbene into the catalyst structure. As illustrated in Scheme 7 (Method C), its reaction with a $^{R}PN^{H}P$ ligand can lead to a neutral or cationic pincer complex depending on the solvent used [63].

3.1.2 Hydrogenation of Esters, Ketones, and Their Derivatives

Both **Ru-MACHO** and **Ru-MACHO-BH** are commercially available, and among the complexes shown in Scheme 7, they are the most extensively studied ones for catalytic hydrogenation reactions. In 2012, Takasago International Corporation reported that **Ru-MACHO** mixed with NaOMe was effective for hydrogenation of esters to alcohols (Eq. 1) [54]. The catalytic system is amenable to benzyloxy,

piperidinyl, or *l*-menthoxy group at the α-position but problematic with methoxy or dimethylamino group at the β-position (e.g., $MeOCH_2CH_2CO_2Me$ and $Me_2NCH_2CH_2CO_2Me$). Most remarkably, hydrogenation of methyl (*R*)-lactate can be performed at room temperature on a multiton scale with minimal erosion to the optical purity (Eq. 2).

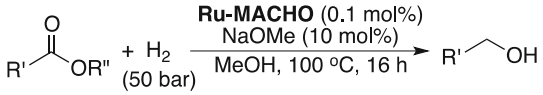

(1)

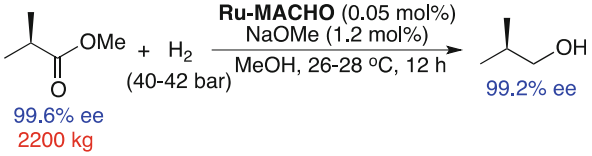

(2)

In a subsequent report [21], Ikariya demonstrated that **Ru-MACHO** was efficient in catalyzing hydrogenation of α-difluorinated esters with turnover numbers (TONs) as high as 20,000 (Eq. 3). Functional groups tolerated in this transformation include C=C bonds (terminal or internal), α-pyridyl, and α-thienyl rings. In addition to **Ru-MACHO**, ^{Ph}**RuH$_2$** and *trans*-(^{Ph}PN^{H}P)$RuCl_2(CO)$ are also capable of catalyzing the hydrogenation reactions, although the dichloride complex displays a lower reactivity. For certain substrates (R′ = H, F, Cl, CF_3), the hydrogenation process can be stopped at the hemiacetal stage, and in general the selectivity for $R'CF_2CH(OH)OR''$ is improved by lowering the H_2 pressure, temperature, and/or the amount of NaOMe. α-Monofluorinated esters can also be hydrogenated under the catalytic conditions; however, the fluorinated primary alcohol products partially undergo cyclization to form epoxides. In a closely related study [64], Lazzari and Cassani showed similar results with R_fCO_2Me (R_f = C_3F_7 or C_5F_{11}), which led to the isolation of highly fluorinated primary alcohols (Eq. 4).

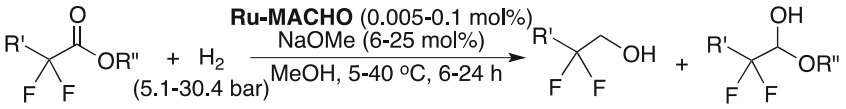

(3)

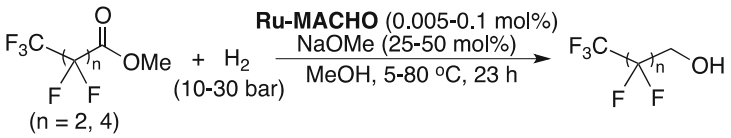

(4)

Another application of the ruthenium-catalyzed ester hydrogenation reactions is in the synthesis of the fragrance hydroxyambran (or 2-cyclododecylpropan-1-ol) [65]. As shown in Scheme 8, hydrogenation of the isomeric mixture of esters with 10% Pd/C provides ethyl 2-cyclododecylpropanoate by saturating all C=C bonds.

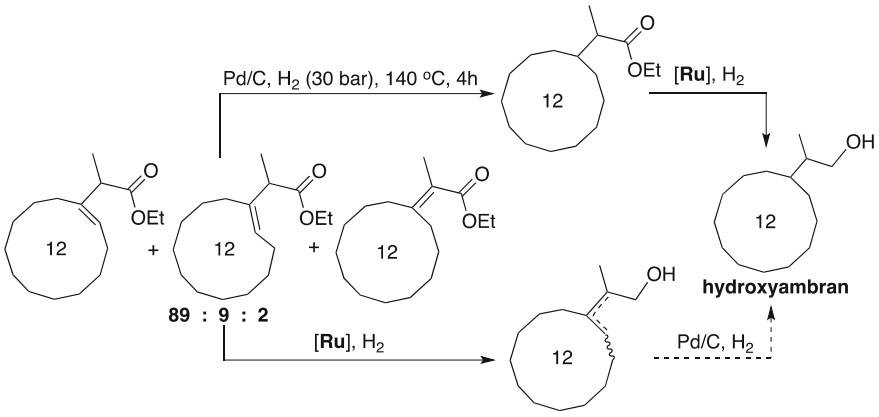

Scheme 8 Synthesis of hydroxyambran via hydrogenation reactions

The second step for ester hydrogenation can be catalyzed at 180°C in toluene by **Ru-MACHO** (0.2 mol%) in conjunction with NaOMe (2 mol%) or at 150°C in diglyme by **Ru-MACHO-BH** (1 mol%) alone, both under 50 bar H_2. The homogeneous ester hydrogenation can be performed first, although hydrogenation of the resulting mixture of alcohols with 10% Pd/C is plagued by deoxygenation.

In collaboration with Procter & Gamble Company, we studied the hydrogenation of fatty acid methyl esters (FAMEs) under neat conditions [66]. Starting from FAMEs derived from coconut oil, fatty alcohols can be obtained in high yields when the hydrogenation reaction is catalyzed at 135°C by **Ru-MACHO** (0.07–1.1 mol%, n_{NaOMe}/n_{Ru} ~9, 35.5–52.7 bar H_2) or **Ru-MACHO-BH** (0.13–1.0 mol%, 35.5–69.9 bar H_2). The catalytic reaction with **Ru-MACHO** and NaOMe has also been conducted on the kilogram scale with a TON of 1860. Direct hydrogenation of coconut oil to fatty alcohols is feasible under base-free conditions, which involve **Ru-MACHO-BH** (2.6–2.8 wt%) operating at 135°C under 52.7 bar H_2. Hydrogenation of FAMEs containing C=C bonds is more challenging, likely due to the presence of peroxide impurities. Dumeignil and Gauvin recently developed a purification procedure involving 18 h of treatment of FAMEs with basic alumina followed by drying with 3 Å molecular sieves for 48 h [67]. The prepurified FAMEs can undergo smooth hydrogenation to fatty alcohols catalyzed by **Ru-MACHO-BH** or ^{iPr}**RuHBH$_4$** (Eq. 5). Depressurizing the system and then reheating the reaction mixture to 130°C under N_2 offers a one-pot, two-step synthesis of wax esters. It should be noted that, compared to **Ru-MACHO-BH**, the isopropyl derivative ^{iPr}**RuHBH$_4$** shows slightly higher catalytic activity in both hydrogenation and dehydrogenation steps and substantially higher overall selectivity for wax esters.

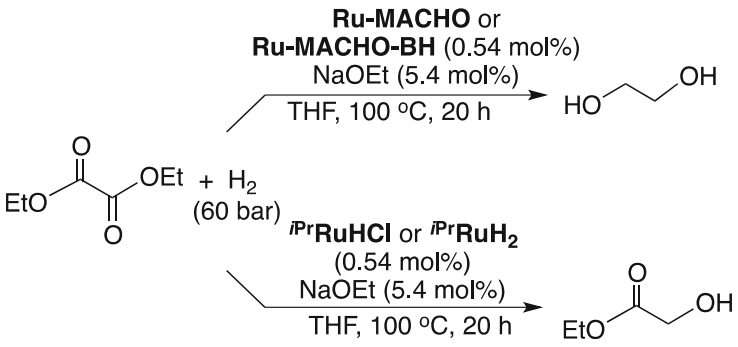

Scheme 9 Complete and partial hydrogenation of diethyl oxalate

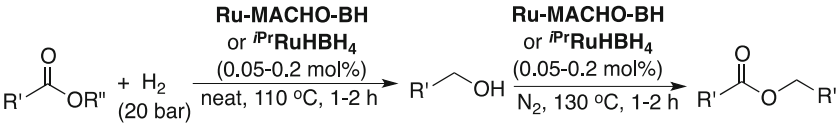

(5)

In 2016, Ogata and Kayaki developed a series of NHC-ligated ruthenium PNP-type catalysts for ester hydrogenation that operate under milder conditions [63]. In particular, complexes **^{Ph}RuCl$_2$(NHC)** and **^{Ar}RuCl$_2$(NHC)** outperform **Ru-MACHO** in hydrogenating methyl benzoate at 80°C under 10 bar H_2. Further optimization of the catalytic conditions showed that in the presence of KO^{t}Bu or NaOMe, **^{Ph}RuCl$_2$(NHC)** was active at 50°C even under a balloon pressure of H_2, converting various esters to the corresponding alcohols (Eq. 6).

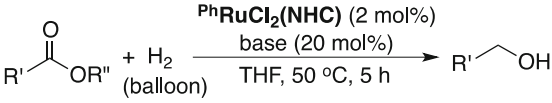

(6)

Dialkyl oxalates belong to a special class of esters for which hydrogenation of the first carbonyl group significantly impacts the reactivity of the remaining carbonyl group. A 2013 report by Beller demonstrated that hydrogenation of diethyl oxalate with **Ru-MACHO** or **Ru-MACHO-BH** in the presence of NaOEt yielded ethylene glycol exclusively (Scheme 9) [68]. Interestingly, replacing the catalyst with **^{iPr}RuHCl** or **^{iPr}RuH$_2$** under otherwise the same conditions afforded ethyl glycolate only. Further investigation of **Ru-MACHO-BH** under base-free conditions suggested that the hydrogenation process could stop at the glycolate stage under a lower temperature (60°C) and after a shorter reaction time (1 h). These results imply that the second hydrogenation step is more difficult. As another example of **Ru-MACHO-BH** differentiating the reactivity of two ester functionalities, MeOCOCH$_2$CO$_2$^{t}Bu was subjected to similar hydrogenation conditions (0.54 mol % [**Ru**], 5.4 mol% NaOEt, 60 bar H_2, 100°C, in THF, 3 h), resulting in a partial hydrogenation product with the sterically more hindered carbonyl group left

Scheme 10 Hydrogenation of α-keto esters

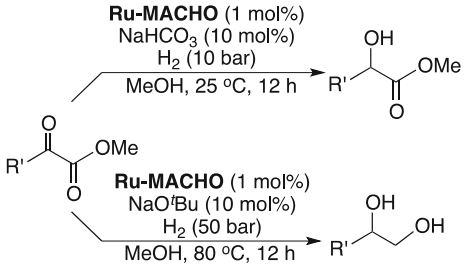

unreacted (i.e., $HOCH_2CH_2CO_2{}^tBu$ as the product) [68]. A closely related substrate is the oxamate illustrated in Eq. 7. The hydrogenation reaction was carried out under more demanding conditions, which unsurprisingly led to complete hydrogenation to ethylene glycol [69].

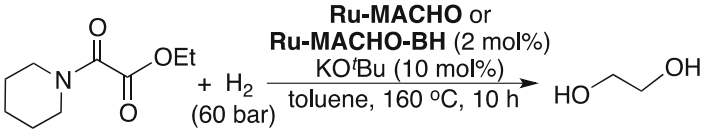

(7)

Given the higher electrophilicity of the carbonyl carbons, ketones should be more readily hydrogenated than esters. Thus, for molecules containing both ketone and ester functionalities, it is possible to fine-tune the reaction conditions so that one or both carbonyl groups are hydrogenated. This was demonstrated by Tang and Xiao in their study of **Ru-MACHO**-catalyzed hydrogenation of α-keto esters [70]. Using $NaHCO_3$ as the base additive paired with relatively low H_2 pressure (10 bar) and temperature (25°C) leads to α-hydroxy esters almost exclusively (Scheme 10). In contrast, using a stronger base NaO^tBu and raising the H_2 pressure to 50 bar and temperature to 80°C result in 1,2-diols with high selectivity (86–100%). Selective hydrogenation of γ-keto esters, in principle, could generate γ-hydroxy esters in an analogous way, although the base additive required for catalyst activation also promotes intramolecular transesterification. Very recently, Paixão and Nielsen reported such conversion with TONs of up to 7,400 by employing **Ru-MACHO** as the precatalyst and NaOEt as the base (Eq. 8) [71]. Under similar conditions, the related ruthenium complexes including **Ru-MACHO-BH**, ^{Ph}**RuH$_2$**, and the commercially available ^{iPr}**RuHCl** also catalyze the hydrogenation of ethyl levulinate to γ-valerolactone, albeit less effectively.

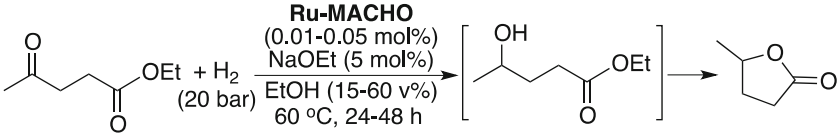

(8)

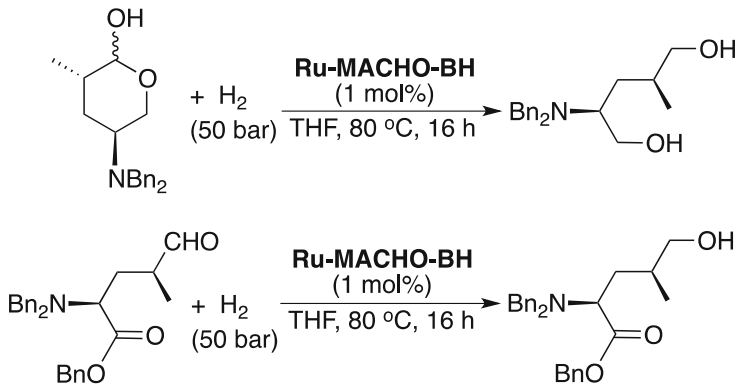

Scheme 11 Hydrogenation of α-chiral hemiacetals and aldehydes

Incorporating a chiral $^{R}PN^{H}P$ ligand into the catalyst structure should allow ketones to be hydrogenated enantioselectively. In a recent report, Junge and Beller tested the catalytic activities of ^{R*}**RuHCl** (*syn*/*anti* mixture or pure *anti* isomer) in hydrogenation of acetophenone and cyclohexyl methyl ketone (Eq. 9) [58]. While the conversion is quantitative, the enantioselectivity is low, suggesting room for improvement in future ligand screening.

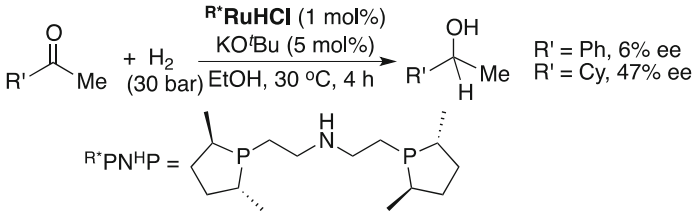

(9)

Since hemiacetals and aldehydes are intermediates during ester hydrogenation, they can be readily reduced to alcohols under the hydrogenation conditions optimized for esters. Obviously, many other transition metal complexes can also catalyze this process. Employing **Ru-MACHO-BH** as the hydrogenation precatalyst has some advantage due to the fact that a base additive is not needed, which is ideal for base-sensitive substrates. In exploring precursors to the new antibiotic nemonoxacin, Clarke used this specific ruthenium complex to catalyze the hydrogenation of a hemiacetal and an aldehyde made from asymmetric hydroformylation reactions [72]. Under the conditions outlined in Scheme 11, the alcohol products are obtained with retention of stereochemistry. It is interesting to note that the ester functionality is intact during the hydrogenation process.

In addition to esters, ketones, hemiacetals, and aldehydes, amides have also been explored as substrates for the ruthenium-catalyzed hydrogenation reactions, although the conditions are much harsher. In 2018, Tu reported the hydrogenation of lactams to amino alcohols catalyzed by **Ru-MACHO-BH** (Eq. 10) [73]. The high

temperature of 150°C is critical to the success of the hydrogenation process. According to the catalyst activation mechanism (Scheme 3), a base additive is normally not needed for **Ru-MACHO-BH** to be catalytically active. In fact, **Ru-MACHO-BH** does show some catalytic activity for hydrogenating *N*-phenyl-2-pyrrolidone. However, the addition of K_3PO_4 significantly enhances the catalytic efficiency (96% vs. 64% yield). The NHC-ligated complex ^{Ph}**RuCl$_2$(NHC)** displays slightly lower activity (82% yield), whereas the methylated PNP pincer complexes (^{Ph}PN^{Me}P)RuHCl(CO) and (^{Ph}PN^{Me}P)RuH(BH_4)(CO) (^{Ph}PN^{Me}P = MeN($CH_2CH_2PPh_2)_2$) are completely inactive, suggesting the importance of the NH moiety. Under similar conditions, hydrogenation of unprotected lactams (e.g., caprolactam and azocan-2-one) and oxazolidinones (e.g., 3-phenyloxazolidin-2-one) is also possible, providing the corresponding amino alcohols in high yields.

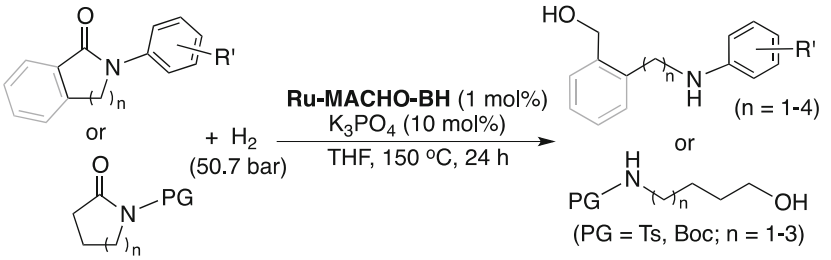

(10)

3.1.3 Hydrogenation of Other Bonds

Substrates that can be hydrogenated with the aforementioned ruthenium catalysts go beyond those containing carbonyl groups. Very recently, Gunanathan showed that **Ru-MACHO** along with KO^{t}Bu was effective and selective for the hydrogenation of epoxides to secondary alcohols (Eq. 11) [74]. This transformation proceeds via direct hydrogen transfer from the presumed active species ^{Ph}**RuH$_2$** rather than by a two-step process involving epoxide-to-ketone isomerization followed by ketone hydrogenation. Functional groups compatible with the catalytic conditions are very similar to those observed in ester hydrogenation, except that herein terminal C=C bonds are also hydrogenated. Hydrogenation of chiral epoxide *R*-glycidol, however, gives a complex mixture, perhaps due to the interference by KO^{t}Bu. Another limitation of the catalytic system is that internal epoxides resist hydrogenation.

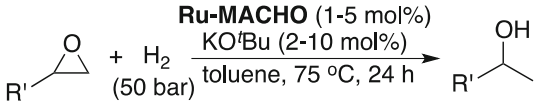

(11)

The strategy of using the ruthenium-based PNP pincer complexes for hydrogenation reactions has been extended to nitrile reduction. Two reports on this topic appeared in 2015, but featured different $^{R}PN^{H}P$ ligands. Both **Ru-MACHO** and **Ru-MACHO-BH** were shown by Beller to catalyze the hydrogenation of nitriles to primary amines, although the former required KO^{t}Bu to activate the catalyst [75]. One of the challenges for nitrile hydrogenation is selectivity, as the intermediates can be trapped by the initially produced primary amines, which lead to secondary amines, secondary imines, and/or tertiary amines as by-products. Under the conditions summarized in Eq. 12, a variety of aliphatic and aromatic nitriles are converted to primary amines with high selectivity. Lowering the temperature or catalyst loading or hydrogenating long-chain nitriles such as dodecanenitrile, however, erodes selectivity for the primary amines. The catalytic system exhibits high functional group tolerance including the preservation of ester functionalities. Substrates that fail to react include furan-2-carbonitrile, 2-methyl-3-butenenitrile, and 6-bromohexanenitrile. Prechtl focused on the study of ruthenium complexes supported by the more bulky ligand $^{t\mathrm{Bu}}PN^{H}P$. Hydrogenation of benzonitrile and *p*-tolunitrile catalyzed by **$^{t\mathrm{Bu}}$RuH$_2$(H$_2$)/$^{t\mathrm{Bu}}$RuH(H$_2$)** or **$^{t\mathrm{Bu}}$RuH** was optimized to favor the secondary imines (Eq. 13), although hydrogenation of *p*-bromobenzonitrile suffered from moderate yield and low selectivity, and hydrogenation of heptyl cyanide catalyzed by **$^{t\mathrm{Bu}}$RuH$_2$(H$_2$)/$^{t\mathrm{Bu}}$RuH(H$_2$)** afforded predominantly octylamine [76]. Under similar catalytic conditions, externally added amines can trap the primary imine intermediates, leading to efficient hydrogenative coupling of nitriles to secondary imines (Eq. 14). Finally, switching the solvent from toluene to ^{i}PrOH and raising the temperature from 50°C to 90°C render **$^{t\mathrm{Bu}}$RuH** more selective for the formation of primary amines (Eq. 15). However, varying amounts of R′CH$_2$N=CMe$_2$ (0–29%) were also observed due to dehydrogenation of the solvent ^{i}PrOH to acetone.

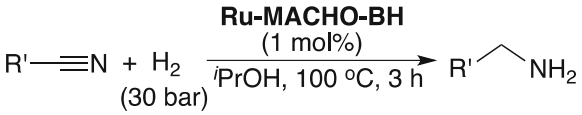

(12)

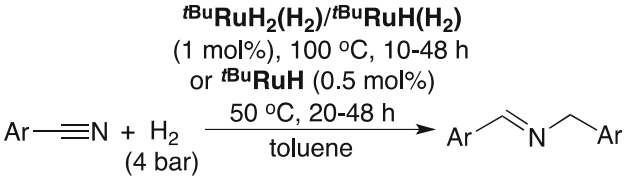

(13)

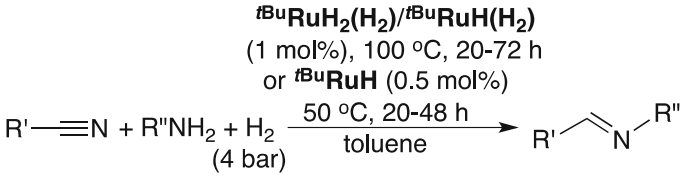

(14)

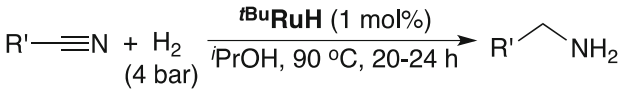

(15)

For the reactions shown in Eqs. 13 and 14, a small amount of secondary amines was often detected, suggesting that it is possible to develop ruthenium-catalyzed hydrogenation of imines. In 2017, Tang reported such process with an objective to develop a diastereoselective route to convert chiral α-ketimino esters to chiral aryl glycine derivatives [77]. As illustrated in Eq. 16, at 25–40°C, **Ru-MACHO** in combination with NaOEt is effective for the C=N bond hydrogenation, which provides *N-tert*-butylsulfinyl-protected α-amino esters with high diastereoselectivity.

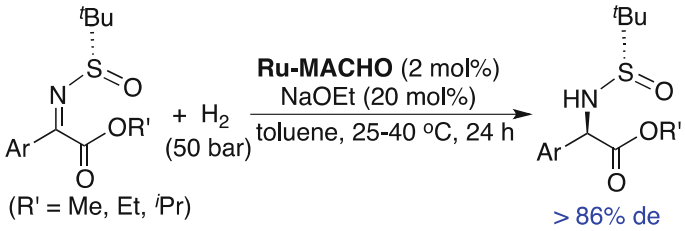

(16)

3.1.4 Hydrogenation Reactions Related to CO_2 or CO Reduction

Homogeneous hydrogenation of CO_2 or CO to liquid fuels such as methanol has been subject to extensive studies in recent years, which, to some degree, is propelled by the development of PNP-type hydrogenation catalysts. Conversion of CO_2 to methanol is formally a six-electron reduction process, and each hydrogenation event reduces formal oxidation state of the carbon by two. Based on this analysis, reduction of CO to methanol is formally a four-electron reduction process. Conversion of CO_2 or CO to oxalate or ethylene glycol requires odd number of electrons to be transferred (Fig. 3), which usually involves a radical intermediate or a process separate from hydrogenation. For a more systematic discussion, hydrogenation reactions described in this section are organized based on how formal oxidation state of the carbon changes: (A) +4 to +2, (B) +2 to −2, (C) +2 to +3 to −1, and (D) +4 to −2.

Hydrogenation of CO_2 to formic acid in organic solvents is an endergonic process ($\Delta G^0_{298} = +32.8$ kJ mol^{-1}). The thermodynamics can be improved by performing

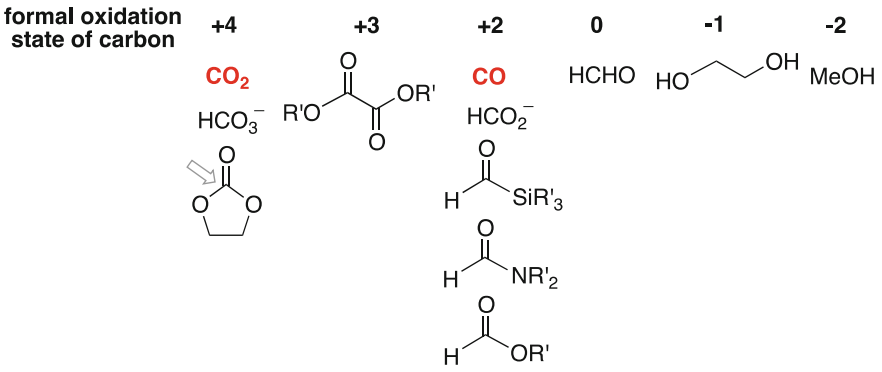

Fig. 3 Compounds relevant to CO_2 or CO reduction

the reaction in water ($\Delta G^0_{298} = -4.0$ kJ mol^{-1}) and/or adding a base to convert formic acid to a formate salt [78]. Direct hydrogenation of bicarbonate to formate is also thermodynamically favorable. For PNP-type catalytic systems, Beller reported in 2014 that transfer hydrogenation of HCO_3^- (or CO_2) to HCO_2^- with MeOH was efficiently catalyzed by **Ru-MACHO** or $^{i\mathrm{Pr}}$**RuHCl** in an alkaline solution [79]. It was noted that hydrogen pressure was built up during the reaction, consistent with catalytic methanol dehydrogenation. To confirm that the in situ generated H_2 was responsible for bicarbonate reduction, **Ru-MACHO** was tested as a hydrogenation catalyst for $NaHCO_3$, which, under the conditions outlined in Eq. 17, afforded HCO_2Na in 71% yield. A more recent report by Treigerman showed that this hydrogenation process could be conducted at 70°C in ^{i}PrOH-H_2O mix solvent and the catalyst could be reused at least three times with an overnight rest of the catalyst between two consecutive runs [80]. Czaun, Prakash, and Olah carried out a more detailed study of **Ru-MACHO**- and **Ru-MACHO-BH**-catalyzed hydrogenation of bicarbonate (Eq. 18) as well as hydrogenation of CO_2 assisted by a hydroxide (Eq. 19) or a carbonate (Eq. 20) [81]. The reverse reaction, dehydrogenation of formate, was also catalyzed by **Ru-MACHO** or **Ru-MACHO-BH**. To demonstrate the reversible hydrogen storage in formate salts, **Ru-MACHO-BH** was employed to catalyze CO_2 hydrogenation (75 bar, p_{H2}: $p_{CO2} = 3$: 1) in the presence of NaOH followed by dehydrogenation under an atmospheric pressure, a process that was repeated at 70°C for six times without a significant loss of the catalytic activity. Interestingly, the NH moiety is not needed here; ($^{\mathrm{Ph}}$PN$^{\mathrm{Me}}$P)RuHCl(CO) catalyzes the hydrogenation and the dehydrogenation reactions with a comparable or better efficiency than **Ru-MACHO** and **Ru-MACHO-BH**.

$$\mathrm{NaHCO_3} + \underset{(10\ \mathrm{bar})}{\mathrm{H_2}} \xrightarrow[\mathrm{MeOH,\ 100\ ^oC,\ 20\ h}]{\textbf{Ru-MACHO}\ (0.05\ \mathrm{mol\%})} \underset{\mathrm{TON = 1420}}{\mathrm{HCO_2Na}} \qquad (17)$$

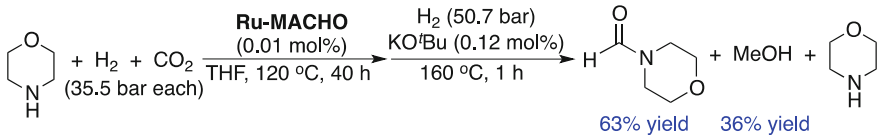

Scheme 12 One-pot, two-step hydrogenation of CO_2 to methanol

$$MHCO_3 + H_2 \xrightarrow[\text{(40 bar)}]{\substack{\textbf{Ru-MACHO} \text{ or} \\ \textbf{Ru-MACHO-BH} \text{ (0.08 mol\%)} \\ \text{THF-}H_2O\text{, 70-80 °C, 0.5-2 h}}} HCO_2M \quad \text{(M = Na, K)} \quad \text{TON: 938-1175} \tag{18}$$

$$MOH + H_2 + CO_2 \xrightarrow[\text{(30 bar each)}]{\textbf{Ru-MACHO-BH} \text{ (0.08 mol\%)} \\ \text{THF-}H_2O\text{, 75-76 °C, 0.5-5 h}} HCO_2M \quad \text{(M = Li, Na, K)} \quad \text{TON: 1000-1160} \tag{19}$$

$$M_2CO_3 + H_2 + CO_2 \xrightarrow[\text{(38 bar) (12 bar)}]{\textbf{Ru-MACHO-BH} \text{ (0.08 mol\%)} \\ \text{THF-}H_2O\text{, 79-85 °C, 63-83 min}} HCO_2M \quad \text{(M = Na, K)} \quad \text{TON: 1750-2164} \tag{20}$$

Hydrogenation of CO_2 along with a primary or secondary amine to generate a formamide is also a formally two-electron reduction process (+4 to +2 for the change in formal oxidation state of the carbon). In 2015, Ding reported that in the presence of KO^{t}Bu (0.1 mol%), **Ru-MACHO**, **^{iPr}RuHCl**, **^{Cy}RuHCl**, **^{Ad}RuHCl**, **^{tBu}RuHCl**, and the methylated complex (^{Ph}PN^{Me}P)RuHCl(CO) were all effective in catalyzing *N*-formylation of morpholine under H_2 and CO_2 (35.5 bar each, 0.1 mol% [Ru], 120°C, in THF) [82]. Using Me_2NH as the amine (also as a base) and lowering the catalyst loading of **Ru-MACHO** to 0.000093 mol% produced DMF with TONs of up to 599,000. The catalyst showed remarkably high stability under the catalytic conditions. With a catalyst loading of 0.002 mol%, **Ru-MACHO** was reused 11 times without the concern for a brief exposure to air between runs. Further hydrogenation of formamides to methanol (formal oxidation state change from +2 to −2) is possible but needs to be performed under a higher temperature and in the presence of KO^{t}Bu. As illustrated in Scheme 12, *N*-formylation of morpholine followed by hydrogenation of the resulting formamide in the same reactor produces methanol in 36% yield along with the unreacted formamide.

Another example of changing formal oxidation state of the carbon from +2 to −2 involves catalytic hydrogenation of silyl formates to methanol. A recent report by Hong showed that silyl formates were first prepared from silanes and CO_2 catalyzed by $Rh_2(OAc)_4$-K_2CO_3 or $RuCl_3$•H_2O [83]. The subsequent hydrogenation reactions can be catalyzed by **Ru-MACHO** combined with KO^{t}Bu but more efficiently by **Ru-MACHO-BH**, which does not require a base. Under the optimized conditions (Eq. 21), various silyl formates (R'_3Si = trialkyl, aryldialkyl, and alkyldiaryl groups) are converted to methanol and the corresponding silanols. Hydrogenation of silyl formates bearing an electron-donating aryl group (e.g., $R'_3Si = Me_2(p\text{-}MeOC_6H_4)Si$

or $Me_2(p\text{-}MeC_6H_4)Si$) under 10 bar H_2 is complicated by the formation of R'_3SiOMe and $R'_3SiOSiR'_3$ as the by-products. The selectivity for methanol and silanols can, however, be improved by raising the H_2 pressure to 80 bar or by adding 0.1 equiv. of methanol. For the latter strategy, methanol attacks silyl formates to yield silanols and methyl formate, which is in turn readily hydrogenated to 2 equiv. of methanol under the catalytic conditions.

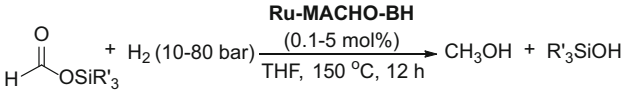

(21)

When K_3PO_4 is used as the catalyst, secondary amines can react with CO (30 bar) at 140°C to give formamides. This reaction coupled with formamide hydrogenation provides an indirect route of hydrogenation of CO to methanol. The challenge lies in the fact that the carbonylation step is favored by an alcoholic solvent, whereas the hydrogenation step is favored by a relatively nonpolar solvent such as toluene. To solve this problem, Prakash designed a one-pot, two-step process in which carbonylation of piperidine or diethylenetriamine (DETA) was carried out in ethanol first [84]. A ruthenium catalyst (**Ru-MACHO** or **Ru-MACHO-BH**), toluene, and H_2 were then added to the reactor, and following hydrogenation, methanol was produced in 75–80% yield. Direct hydrogenation of CO to methanol was made possible by using DETA as the amine and toluene-EtOH (1:1) as the mix solvent (Eq. 22). The reaction was performed in a closed system, providing methanol in 59% yield (or a TON of 539 based on the amount of **Ru-MACHO-BH** used) along with formamides in 15% yield.

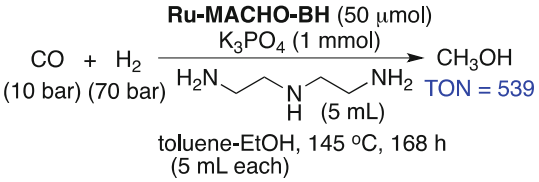

(22)

Similarly, palladium-catalyzed oxidative carbonylation of piperidine provides an oxamide that can be hydrogenated to ethylene glycol, representing an indirect method of hydrogenating CO to ethylene glycol. The overall process involves changes of formal oxidation state of the carbon from +2 to +3 and then to −1. To this end, Li and Beller reported in 2016 that oxidative carbonylation of piperidine was best catalyzed by $Pd(acac)_2$-$P(o\text{-}tol)_3$ using compressed air as the source of oxidant [85]. Hydrogenation of the resulting oxamide is affected by **Ru-MACHO** or **Ru-MACHO-BH** (0.1–1 mol% loading, in toluene) at 160°C under 60 bar H_2 using KO^tBu (2–10 mol%) as the additive. Combining these two steps in one reactor is difficult, and the exchange of solvents and a filtration through silica gel are required after the formation of the oxamide (Scheme 13).

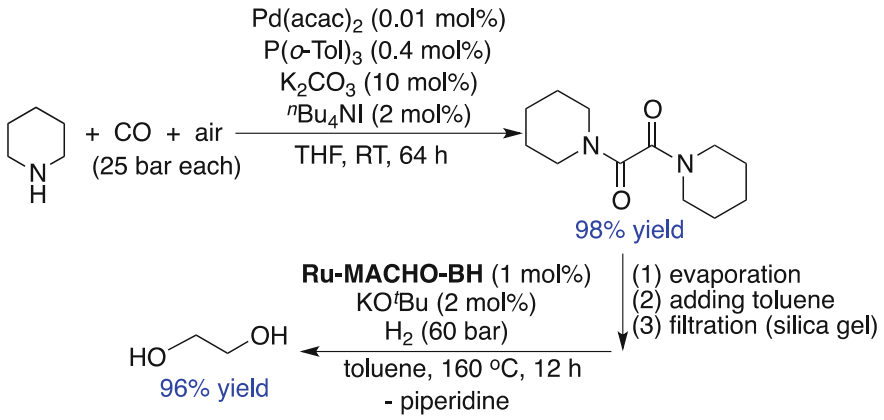

Scheme 13 Piperidine-mediated conversion of CO to ethylene glycol

For the hydrogenation of CO_2 to methanol (with a change of the carbon formal oxidation state from +4 to −2), one strategy is to use cyclic carbonates as surrogates for CO_2, which can bypass formic acid (incompatible with metal hydrides) or formate salts (thermodynamic sinks). This was successfully demonstrated in 2012 by Ding who studied ruthenium-catalyzed hydrogenation of ethylene carbonate [55]. Among the precatalysts screened, **Ru-MACHO** performs significantly better than the analogous complexes bearing alkyl groups as the phosphorus substituents (i.e., $^{i\mathrm{Pr}}$**RuHCl**, $^{\mathrm{Cy}}$**RuHCl**, $^{\mathrm{Ad}}$**RuHCl**, and $^{t\mathrm{Bu}}$**RuHCl**) with TONs as high as 87,000. In this case, the NH moiety is crucial for the catalysis because the methylated complex ($^{\mathrm{Ph}}$PN$^{\mathrm{Me}}$P)RuHCl(CO) fails to hydrogenate ethylene carbonate. Under the optimized conditions (Eq. 23), various cyclic carbonates are converted to diols and methanol in almost quantitative yields. The hydrogenation strategy was further applied to poly(propylene carbonate) with an M_w of 1,000,698, giving 1,2-propylene glycol and methanol in high yield (Eq. 24). Hydrogenation of (*R*)-propylene carbonate under similar conditions generates racemic 1,2-propylene glycol, presumably due to the reversibility of the hydrogenation process.

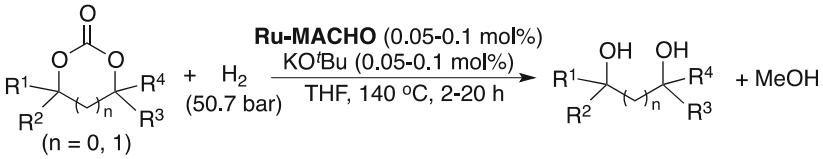

(23)

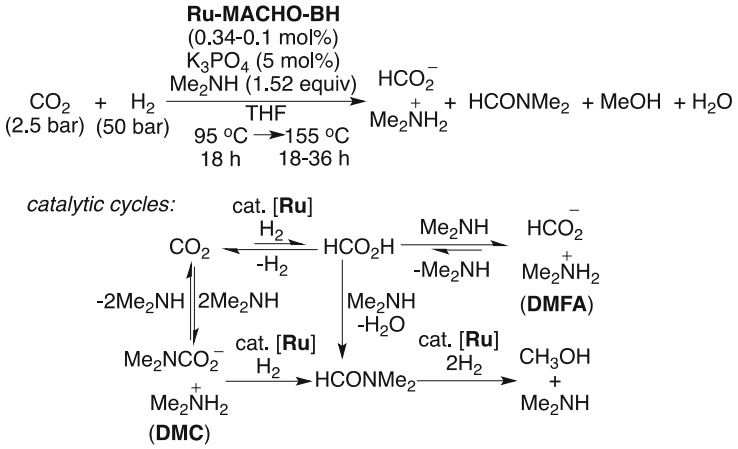

Scheme 14 Ruthenium-catalyzed hydrogenation of CO_2 in the presence of Me_2NH

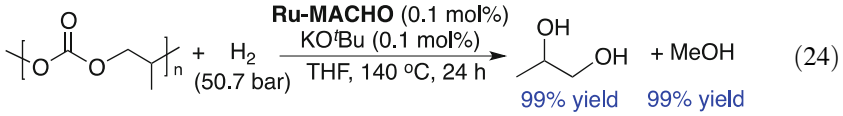

(24)

The seminal work by Sanford in 2015 demonstrated that direct catalytic hydrogenation of CO_2 to methanol could be accomplished via tandem catalysis of Me_2NH promoted by **Ru-MACHO-BH** (Scheme 14) [86]. The proposed mechanism involves equilibrium between CO_2 and dimethylammonium dimethylcarbamate (DMC), which can be hydrogenated to formic acid (trapped as dimethylammonium formate or DMFA) and DMF, respectively. The most challenging step is the hydrogenation of DMF to methanol, a process requiring temperatures as high as 155°C. Under such conditions, the ruthenium catalyst also starts to decompose. To maximize the yield for methanol, a temperature ramp strategy was developed so that a sufficient amount of DMF and DMFA could be accumulated at 95°C. The subsequent hydrogenation carried out at 155°C provides methanol with TONs of up to 550 and DMF-DMFA with combined TONs of up to 1870.

In addition to Me_2NH, polyamines can also be employed to assist CO_2 hydrogenation. Olah and Prakash reported in 2016 that pentaethylenehexamine (PEHA) combined with a catalytic amount of **Ru-MACHO** or **Ru-MACHO-BH** promoted the hydrogenation of CO_2 to methanol in an etherate solvent (e.g., THF, 1,4-dioxane, diglyme, or triglyme) [87]. After extensive optimization of the reaction, it was determined that with this new catalytic system, the temperature ramp strategy and the addition of K_3PO_4 were unnecessary. At 155°C under 75 bar H_2/CO_2 (3: 1 or 9: 1), methanol was obtained with TONs of up to 1,200 and the catalyst was reused five times with 75% of the initial activity retained. CO_2 can also be captured from simulated air (400 ppm of CO_2 in 80% N_2 and 20% O_2) by an aqueous solution of

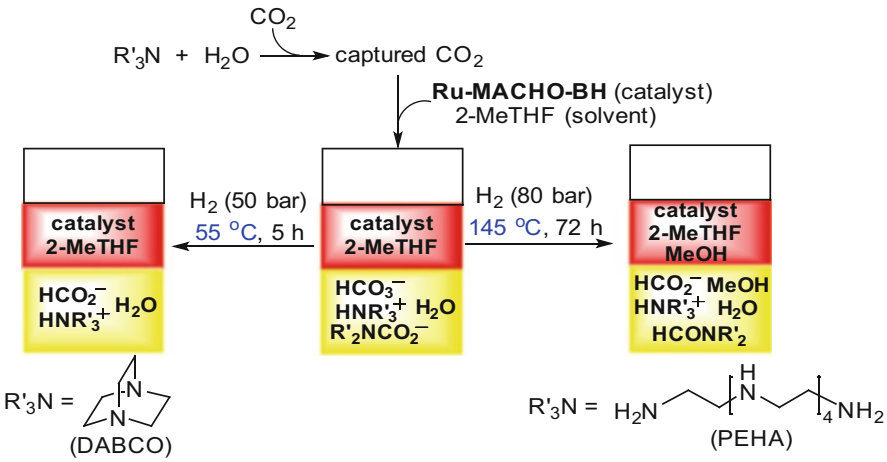

Scheme 15 CO_2 capture and the subsequent hydrogenation reaction in a biphasic mixture

PEHA and then subjected to hydrogenation conditions (155°C, 50 bar H_2, **Ru-MACHO-BH** as the catalyst, 55 h), which provides methanol in 79% yield.

Additional improvements to the catalytic system include hydrogenation of the captured CO_2 (from pure CO_2 or simulated air) using various polyamines in a biphasic mixture of water and 2-methyltetrahydrofuran (2-MeTHF). This allows an easy separation of the catalyst (in 2-MeTHF layer) from the hydrogenation products (in water layer). Depending on the temperature applied, the hydrogenation product can be a formate salt [88] or predominantly methanol [89] (Scheme 15). Both processes have shown excellent recyclability of the catalyst (4–5 runs).

The polyamines play important roles in determining the yield and selectivity of the hydrogenation process. For hydrogenation of the captured CO_2 to formate (in 1,4-dioxane, 50°C, 50 or 80 bar H_2), 1,4-diazabicyclo[2.2.2]octane (DABCO), 1,1,3,3-tetramethylguanidine (TMG), and 1,8-diazabicycloundec-7-ene (DBU) outperform PEHA and branched polyethyleneimines (BPEI, $M_w = 800$) in terms of the formate yield [88]. For hydrogenation of the captured CO_2 to methanol (in 2-MeTHF, 145°C, 70 bar H_2), PEHA gives a higher methanol yield than BPEI ($M_w = 800$ or 25,000), linear polyethyleneimines (LPEI, $M_w = 2{,}500$ or 100,000), and poly(allylamine) (PAA, $M_w = 10{,}000$). The latter three polyamines also produce more formate and formamide as the by-products [89]. In a related study, Kayaki also used BPEI ($M_n = 600$) and LPEI ($M_n = 2{,}500$, 5,000, 25,000, or 250,000) to assist CO_2 hydrogenation, although the reactions were carried out in THF only [90]. At 100°C under 100 bar H_2 and 100 bar CO_2, ruthenium complexes including **Ru-MACHO**, **Ru-MACHO-BH**, ^{Cy}**RuHCl**, and ^{Ph}**RuCl$_2$(NHC)** were shown to be similarly effective in converting CO_2 and the polymers to *N*-formylated PEI with 67–90% CHO content. Further hydrogenation of the *N*-formylated PEI to methanol or direct hydrogenation of CO_2 to methanol assisted by BPEI or LPEI is best catalyzed by **Ru-MACHO-BH** at 140–160°C under 80 bar H_2/CO_2 (3:1 or 7:1).

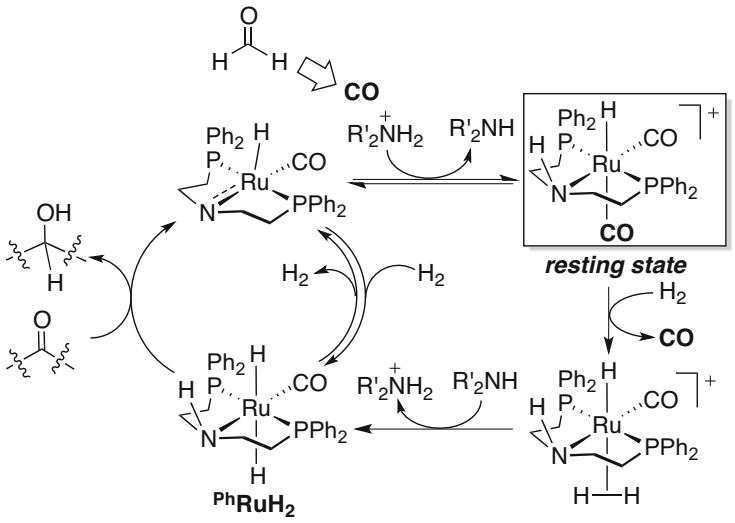

Scheme 16 Involvement of the cationic bis(carbonyl) hydride species during the catalytic hydrogenation reaction

The nature of the phosphorus substituents also plays critical roles in determining the catalytic efficiency. Although **Ru-MACHO**, ^{iPr}**RuHCl**, and ^{Cy}**RuHCl** (in the presence of K_3PO_4) all prove to be active precatalysts for the hydrogenation of formamides to methanol [91, 92], for polyamine-assisted CO_2 hydrogenation, **Ru-MACHO** (or **Ru-MACHO-BH**) appears to be the best choice for maximizing methanol yield [89, 92]. A recent mechanistic study by Prakash offered very insightful information about why the phenyl groups are beneficial for the hydrogenation reaction [92]. Evidently, during CO_2 to methanol conversion, a small amount of CO (~0.2%) is generated, which poisons those ruthenium catalysts bearing alkyl substituents. In fact, during PEHA-assisted CO_2 hydrogenation, the resting state of the catalyst was identified as a cationic bis(carbonyl) hydride complex (Scheme 16). For the phenyl derivative, the CO is more labile due to weaker donation from the phosphorus atoms, allowing $[(^{Ph}PN^{H}Ph)Ru(CO)_2H]^+$ to reenter the catalytic cycle by forming the active species ^{Ph}**RuH$_2$**. Such process is less favorable for the alkyl derivatives.

3.2 Iron Catalysts

3.2.1 Synthesis of (Pre)catalysts

The recent surge in developing base metal catalysis has prompted many research groups to design iron-based hydrogenation catalysts. A logical extension of the work shown in the previous section would be replacing ruthenium with iron, although the

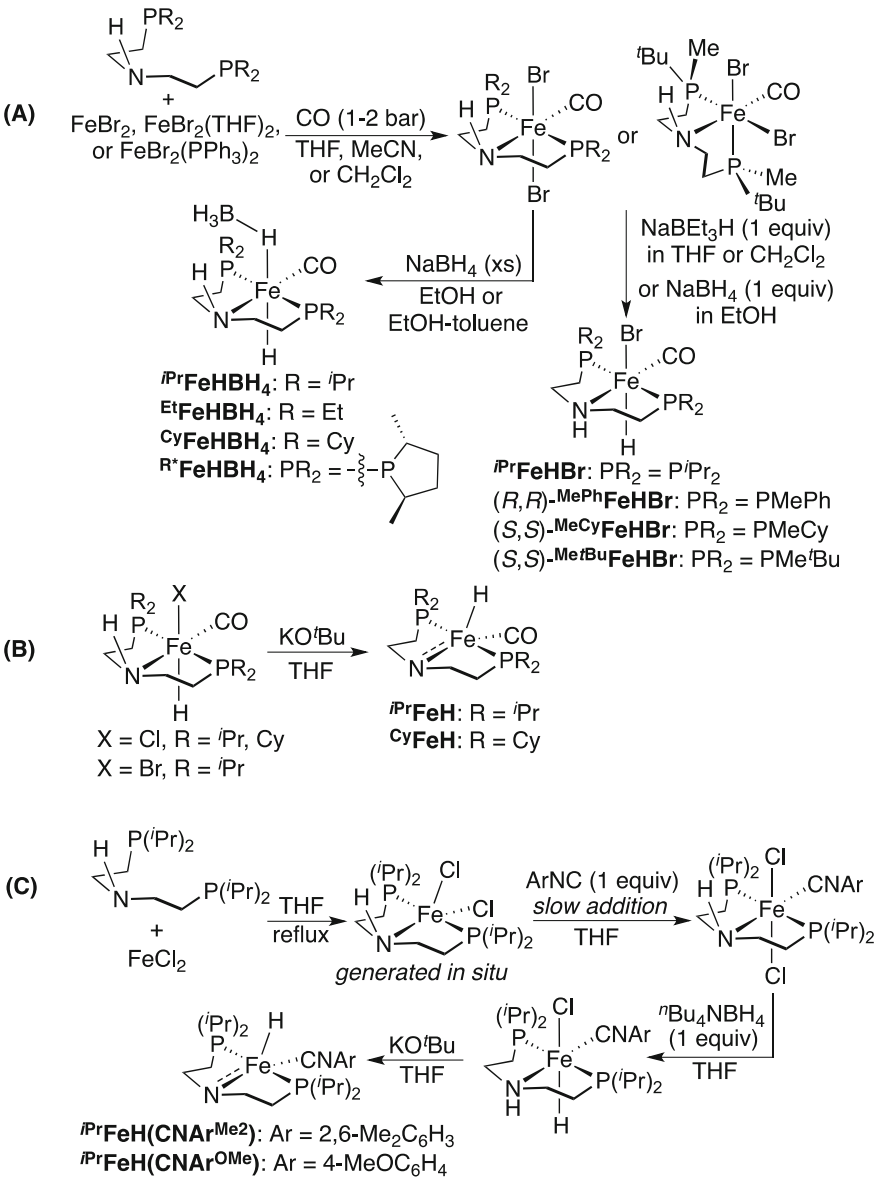

Scheme 17 Synthetic routes to iron-based hydrogenation (pre)catalysts

chemistry of the ruthenium PNP-type complexes cannot be simply extrapolated to the iron systems. This is already reflected by how the iron-based (pre)catalysts are made (Scheme 17). First of all, iron analogs of the ruthenium precursors RuHCl(CO)$(PPh_3)_3$ and Ru(COD)(2-methylallyl)$_2$ do not exist. While the catalysis community enjoys the use of **Ru-MACHO** and **Ru-MACHO-BH**, both of which are

commercially available, **Fe-MACHO** remains elusive, and **Fe-MACHO-BH** has a very limited lifetime in solution [93]. Nevertheless, in 2013, Beller first reported the synthesis of $^{i\mathbf{Pr}}$**FeHBH$_4$**, which involved the treatment of *trans*-($^{i\mathrm{Pr}}$PN$^{\mathrm{H}}$P)FeBr$_2$(CO) (made from $^{i\mathrm{Pr}}$PN$^{\mathrm{H}}$P and FeBr$_2$(THF)$_2$ under 1 bar CO) with excess NaBH$_4$ in EtOH (Scheme 17, Method A) [94]. Reducing the amount of NaBH$_4$ to 1 equiv. led to the isolation of $^{i\mathbf{Pr}}$**FeHBr** [95], which was alternatively prepared in THF from *trans*-($^{i\mathrm{Pr}}$PN$^{\mathrm{H}}$P)FeBr$_2$(CO) using NaBEt$_3$H as the hydride source [94]. Depending on the reaction time and work-up procedures, both $^{i\mathbf{Pr}}$**FeHBH$_4$** and $^{i\mathbf{Pr}}$**FeHBr** can be isolated as a mixture of *syn* and *anti* isomers or as a pure *anti* isomer, although it is expected to have no impact on the catalytic performance. This synthetic strategy has been extended to other ligand systems including $^{\mathrm{Et}}$PN$^{\mathrm{H}}$P [93, 96], $^{\mathrm{Cy}}$PN$^{\mathrm{H}}$P [97, 98], the phospholane-based PNP ligand [58], and the *P*-stereogenic PNP ligands [39]. It is worth pointing out that (*S*,*S*)-(^{t}BuMePCH$_2$CH$_2$)$_2$NH adopts the *facial* coordination mode upon formation of the dibromide complex, whose reaction with NaBEt$_3$H must be carried out in CH$_2$Cl$_2$ instead of THF to avoid degradation. The three *P*-chiral precatalysts, $^{\mathbf{MePh}}$**FeHBr**, $^{\mathbf{MeCy}}$**FeHBr**, and $^{\mathbf{Me}t\mathbf{Bu}}$**FeHBr**, decompose quickly in solution; therefore, they should be prepared right before use [39]. The more commonly used iron precatalyst $^{i\mathbf{Pr}}$**FeHBH$_4$** can also be synthesized from the dichloride complex *trans*-($^{i\mathrm{Pr}}$PN$^{\mathrm{H}}$P)FeCl$_2$(CO) and NaBH$_4$ (10 equiv) in MeCN-EtOH, although applying this protocol to *trans*-($^{\mathrm{Cy}}$PN$^{\mathrm{H}}$P)FeCl$_2$(CO) fails to generate $^{\mathbf{Cy}}$**FeHBH$_4$** cleanly [99].

The five-coordinate complex $^{i\mathbf{Pr}}$**FeH** can be obtained from dehydrohalogenation of $^{i\mathbf{Pr}}$**FeHBr** [100] or $^{i\mathbf{Pr}}$**FeHCl** (made from *trans*-($^{i\mathrm{Pr}}$PN$^{\mathrm{H}}$P)FeCl$_2$(CO) and ^{n}Bu$_4$NBH$_4$) [101] with KO^{t}Bu (Scheme 17, Method B). The cyclohexyl analog $^{\mathbf{Cy}}$**FeH** is also available using this method [101]. Preparing the isocyanide derivatives $^{i\mathbf{Pr}}$**FeH(CNAr$^{\mathbf{Me2}}$)** and $^{i\mathbf{Pr}}$**FeH(CNAr$^{\mathbf{OMe}}$)** follows similar procedures (Method C) [102]. The key challenge here is in the synthesis of *trans*-($^{i\mathrm{Pr}}$PN$^{\mathrm{H}}$P)FeCl$_2$(CNR). To avoid the undesired cationic bis(isocyanide) complexes, isocyanides must be diluted and added slowly to ($^{i\mathrm{Pr}}$PN$^{\mathrm{H}}$P)FeCl$_2$.

3.2.2 Hydrogenation of Esters, Ketones, and Their Derivatives

In 2014, the Beller group [24] and our group [95] independently reported that $^{i\mathbf{Pr}}$**FeHBH$_4$** was effective in catalyzing the hydrogenation of esters including lactones to alcohols (Eq. 25). Functional groups tolerated under the catalytic conditions include CF$_3$, MeO, pyridyl, furyl, benzothiazolyl, and isolated C=C bonds. In contrast, nitrile groups and conjugate C=C bonds are hydrogenated along with the carbonyl groups, and phenol-type functionality shuts down the catalysis completely. For further applications (Fig. 4), $^{i\mathbf{Pr}}$**FeHBH$_4$** has been utilized to catalyze the hydrogenation of a dodecapeptide, which is a precursor to the drug molecule Alisporivir [24], and an industrial sample CE-1270, which is derived from coconut oil and used in surfactant production [95]. As with the ruthenium system, $^{i\mathbf{Pr}}$**FeHBH$_4$** has also been tested for direct catalytic hydrogenation of coconut oil (2.0 wt% catalyst loading, 135°C, 52.7 bar H$_2$), although the fatty alcohol yield is

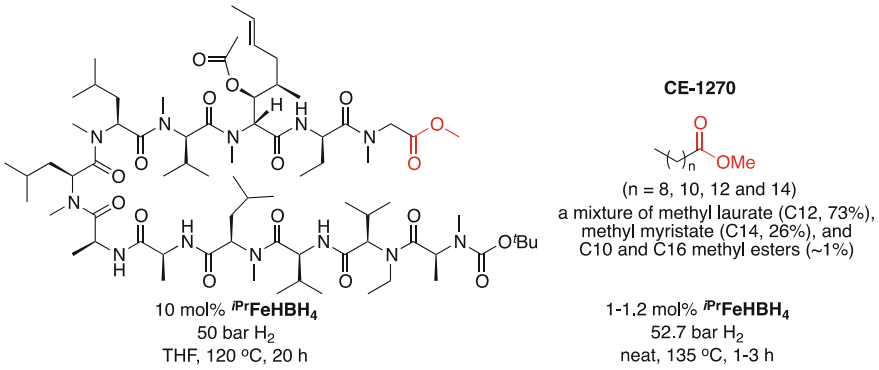

Fig. 4 A dodecapeptide and an industrial sample CE-1270 used in iron-catalyzed hydrogenation reactions

low (12%) due to the low thermal stability of the catalyst as well as its sensitivity toward impurities [66].

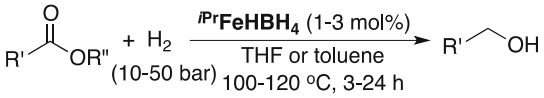

(25)

The complex $^{i\mathrm{Pr}}$**FeHBH$_4$** is a precatalyst; under heating, it releases BH_3 to generate the active species *trans*-($^{i\mathrm{Pr}}$PN$^{\mathrm{H}}$P)$FeH_2(CO)$ [22, 24]. This process can be facilitated by the addition of Et_3N to trap BH_3, resulting in a more efficient catalytic system [22]. However, using other bases such as KO^{t}Bu and Na_2CO_3 can reduce the alcohol yield [24]. In the presence of KO^{t}Bu (or NaOMe) and under H_2, $^{i\mathrm{Pr}}$**FeHBr** is also converted to *trans*-($^{i\mathrm{Pr}}$PN$^{\mathrm{H}}$P)$FeH_2(CO)$, thus catalyzing ester hydrogenation, although it can be complicated by base-promoted transesterification with the alcohol products [95].

To understand the substituent effects, Beller replaced the isopropyl groups in $^{i\mathrm{Pr}}$**FeHBH$_4$** with ethyl or cyclohexyl groups and studied the catalytic performance of these new borohydride complexes [96]. Consistent with the steric argument, at a relatively low temperature of 60°C, $^{\mathrm{Et}}$**FeHBH$_4$** performs better than $^{i\mathrm{Pr}}$**FeHBH$_4$**, which is in turn more reactive than $^{\mathrm{Cy}}$**FeHBH$_4$** for the hydrogenation of methyl benzoate. Notably, $Me_2NCH_2CH_2CO_2Me$, which is not a viable substrate for the **Ru-MACHO** system, can be smoothly hydrogenated to $Me_2N(CH_2)_3OH$ at 100°C under 30 bar H_2 using $^{\mathrm{Et}}$**FeHBH$_4$** as the precatalyst (1 mol%). It should be emphasized here that temperature and H_2 pressure play profound roles in controlling the activation, stability, and reactivity of the borohydride complexes and ultimately their catalytic efficiency. A closely related study by Langer showed a decreasing reactivity order of $^{i\mathrm{Pr}}$**FeHBH$_4$** > $^{\mathrm{Cy}}$**FeHBH$_4$** > $^{\mathrm{Et}}$**FeHBH$_4$** when the hydrogenation of methyl benzoate was conducted as 100°C under 10 bar H_2 (Eq. 26) [93].

Scheme 18 Catalytic hydrogenation of alkyl levulinates

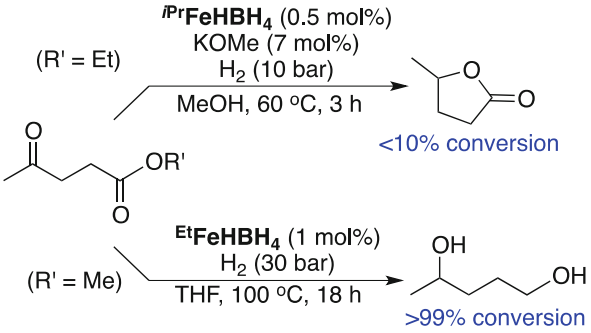

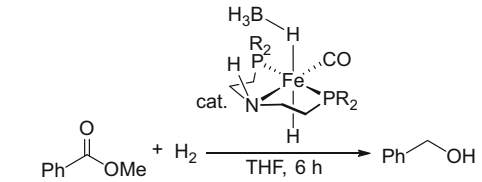

(26)

p_{H2} = 30 bar, 60 °C ^{Et}FeHBH$_4$ > ^{iPr}FeHBH$_4$ > ^{Cy}FeHBH$_4$

p_{H2} = 10 bar, 100 °C ^{iPr}FeHBH$_4$ > ^{Cy}FeHBH$_4$ > ^{Et}FeHBH$_4$

Catalytic hydrogenation of levulinates, which contain two different types of carbonyl groups, has been explored with the iron PNP-type complexes. Very recently, Paixão and Nielsen showed that at 60°C under 10 bar H_2, **^{iPr}FeHBH$_4$** combined with KOMe catalyzed the hydrogenation of ethyl levulinate to γ-valerolactone with <10% conversion in 3 h (Scheme 18) [71]. This level of activity is lower than the analogous ruthenium complexes including **^{iPr}RuHCl** and **Ru-MACHO-BH**. With a catalytic amount of **^{iPr}FeHBr** (0.05 mol%) and a stoichiometric amount of KOH, levulinic acid is also hydrogenated at 100°C under 50.7 bar H_2, giving γ-valerolactone with a TON of 540 in 5 h [103]. Under base-free conditions with **^{Et}FeHBH$_4$** (Scheme 18), methyl levulinate can be fully converted to a diol in high yield [96].

Simple ketones are much more reactive; therefore, their hydrogenation to alcohols can be carried out under milder reaction conditions. For example, hydrogenation of 4-methoxyacetophenone catalyzed by 1 mol% **^{iPr}FeHBH$_4$** or **^{iPr}FeH** alone or by **^{iPr}FeHBr** with 10 mol% KO^{t}Bu takes place at room temperature under 6.5 bar H_2, which affords the alcohol product quantitatively in 8 h [104]. Hydrogenation of acetophenone catalyzed by **^{iPr}FeH** (0.2 mol%) is operative at room temperature under 1 bar H_2 [105].

The chiral precatalysts illustrated in Scheme 17 have been designed specifically for asymmetric hydrogenation of ketones. With the exception of (*S*,*S*)-**^{MetBu}FeHBr**, which, after activation by KO^{t}Bu, fails to catalyze the hydrogenation of acetophenone [39], all other precatalysts promote ketone hydrogenation at 20–40°C under 5.5–50 bar H_2. While the conversions are high, ee's (ee = enantiomeric excess) for the alcohol products are typically low or moderate (0–64%). The

more selective iron-based catalysts for ketone (and imine) hydrogenation are those developed by Morris with chirality built between nitrogen and phosphorus donors. These unsymmetrical P-N^H-P′-type ligand systems are beyond the scope of this review. Interested readers are directed to several recent papers for more details [106–109].

For other carbonyl-based substrates, three research groups have independently investigated iron-catalyzed hydrogenation of amides, which generates amines and alcohols via C–N bond cleavage. In 2016, Langer demonstrated that ^{Et}**FeHBH$_4$** was effective for the hydrogenation of PhCONHR″ (R″ = Ar, Me), $CF_3CONHPh$, $PhCONMe_2$, and γ-lactams bearing an *N*-aryl group (Eq. 27) [93]. Under similar conditions, δ-lactams such as *N*-phenyl-2-piperidone and *N*-bis(trifluoromethyl)-phenyl-2-piperidone failed to be hydrogenated. About the same time, Sanford reported that the addition of a weak base such as K_3PO_4 and Et_3N could enhance the catalytic activity of ^{Cy}**FeHBH$_4$** in amide hydrogenation [97]. Compared to ^{Cy}**FeHBH$_4$**, ^{iPr}**FeHBH$_4$** and ^{Et}**FeHBH$_4$** are less efficient. Under the optimized conditions (Eq. 27), $CH_3CONHPh$, CH_3CONPh_2, PhCONHPh, and $ArCONPh_2$ (Ar = Ph or a more electron-withdrawing aryl group) are converted to the corresponding amines and alcohols in high yields. In contrast, hydrogenation of $PhCONMe_2$ and $CF_3CONHBn$ is low yielding, and hydrogenation of 4-$MeOC_6H_4CONPh_2$ and 4-$Me_2NC_6H_4CONPh_2$ is negligible. In a 2017 report, Bernskoetter employed a low catalyst loading of ^{iPr}**FeH** (0.07 mol%) and performed the reaction at 100°C under 30.4 bar H_2 (in THF), which resulted in TONs of 50–160 in 4 h for the hydrogenation of R′CONHPh (R′ = Me, Ph, CF_3) [110]. The addition of LiOTf and HCONHPh as additives was shown to enhance the catalytic activity of ^{iPr}**FeH**. Under the modified catalytic conditions (Eq. 27), PhCONHMe remains to be unreactive.

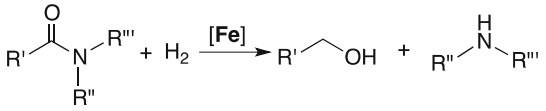

^{Et}**FeHBH$_4$** (2-10 mol%) 50 bar H_2, 70-100 °C THF, 24 h	^{Cy}**FeHBH$_4$** (0.33-4 mol%) K_3PO_4 (1.66-20 mol%) 20-50 bar H_2, 110-130 °C THF, 3 h	^{iPr}**FeH** (0.07 mol%) LiOTf (20 equiv) HCONHPh (20 equiv) 60.8 bar H_2, 120 °C, THF, 16 h
Langer (2016)	**Sanford (2016)**	**Bernskoetter (2017)**

(27)

3.2.3 Hydrogenation of Other Bonds

The iron-based PNP-type complexes are capable of catalyzing the hydrogenation of polar bonds other than the C=O bonds described above. As demonstrated by Beller in 2014, hydrogenation of aromatic and aliphatic nitriles can be catalyzed by ^{iPr}**FeHBH$_4$** at 70–130°C under 30 bar H_2 (Eq. 28) [111]. The catalytic system

shows excellent selectivity for primary amines, which can be conveniently isolated as hydrochloride salts following acidification by HCl. A wide variety of functional groups such as MeO, halogens, NH_2, pyridyl, indolyl, and thienyl are amenable to the catalytic conditions. In contrast, NO_2 and phenol-type groups shut down the reaction. Most remarkably, hydrogenation of 4-$MeOCOC_6H_4CN$ at 130°C is selective for the nitrile functionality despite having a reducible ester group. Hydrogenation of cinnamonitrile followed by acidification produces *trans*-$[PhCH{=}CHCH_2NH_3]Cl$ with the C=C bond almost intact, further highlighting the high chemoselectivity (>25: 1). Here, the presence of the NH moiety is critical to the success of the hydrogenation process. A control experiment using ($^{iPr}PN^{Me}P$)FeH(CO)(BH_4) as the catalyst did not yield any hydrogenation product. In a follow-up study, Beller showed that **^{Cy}FeHBH$_4$** was similarly effective, whereas **^{Et}FeHBH$_4$** became inactive when the catalyst loading was reduced from 1 mol% to 0.5 mol% [98]. According to that study, temperature is very critical for the outcome of the hydrogenation. Hydrogenation of PhCN performed below 70°C leads mainly to the secondary imine $PhCH{=}NCH_2Ph$.

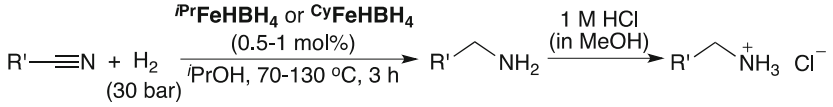

(28)

N-heterocycles have been studied as potential organic hydrogen storage materials through reversible acceptorless dehydrogenation and hydrogenation reactions, both of which require a catalyst. In 2014, Jones reported that **^{iPr}FeHBr**, when activated by KO^{t}Bu, was effective for the hydrogenation of quinoline derivatives to 1,2,3,4-tetrahydroquinaldines (Eq. 29) [100]. Related *N*-heterocycles including 2-methylindole and 2,6-lutidine are also hydrogenated under similar conditions. As expected, **^{iPr}FeHBH$_4$** also serves a precatalyst (without a base additive) for this process, although it is less active, resulting in 89% of quinoline being hydrogenated even at a higher temperature of 110°C. According to DFT calculations by Surawatanawong, the first hydrogenation event converts quinoline to 1,4-dihydroquinoline, which undergoes base-assisted isomerization to 3,4-dihydroquinoline [112]. Further hydrogenation of the C=N bond furnishes the 1,2,3,4-tetrahydroquinaldine product.

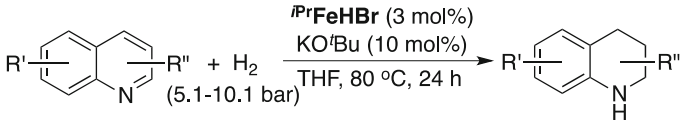

(29)

Typically, olefins are not considered viable substrates for hydrogenation systems that operate via metal-ligand cooperation. However, when the C=C bonds are significantly polarized, they can accept H^- and H^+ from H–M–N–H-type complexes in a similar way as carbonyl groups. In a recent study, Jones demonstrated this

concept in studying iron-catalyzed hydrogenation of styrene and its derivatives [113]. At room temperature under an atmospheric H_2 pressure, styrene is converted to ethylbenzene quantitatively in 24 h when ^{iPr}**FeHBr** (5 mol%) mixed with KO^{t}Bu (15 mol%) or ^{iPr}**FeH** (5 mol%) is employed as the catalyst. The borohydride complex ^{iPr}**FeHBH$_4$** is significantly less active due to the need to remove BH_3, which is usually favored at elevated temperatures. Under the optimized conditions (Eq. 30), substituted styrenes, especially those containing electron-withdrawing groups, undergo C=C bond hydrogenation smoothly. Because the reaction conditions are very mild, other reducible functional groups such as ester, pyridyl, and CN are tolerated, although hydrogenation of 4-cyanostyrene is sluggish due to catalyst inhibition by substrate coordination. Hydrogenation of *trans*-PhCH=CHCOCH$_3$ eventually gives the fully saturated product PhCH$_2$CH$_2$CH(OH)CH$_3$. At the early stage of the reaction, C=O hydrogenation is faster than C=C hydrogenation. Consistent with a mechanism featuring metal-ligand cooperativity, weakly polarized C=C bonds such as those in 1-hexene and *tert*-butylethylene resist hydrogenation, and the methylated complex (^{iPr}PN^{Me}P)FeH(CO)(BH$_4$) shows no catalytic activity even at 100°C.

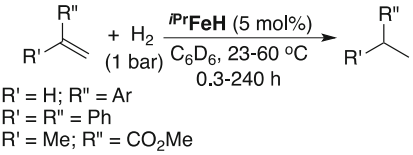

(30)

3.2.4 Hydrogenation Reactions Related to CO_2 or CO Reduction

Combining iron catalysis with CO_2 reduction addresses many sustainability-related challenges [114]. Like the ruthenium-based systems described earlier, iron-based PNP-type complexes have also been explored in variety of transformations that are associated with CO_2 reduction. Once again, the discussion here is organized based on how formal oxidation state of the carbon changes during hydrogenation (Fig. 3).

For an example involving a change of +4 to +2 in carbon oxidation state, Hazari and Schneider showed in 2014 that hydrogenation of CO_2 (1:1 mixture with a total pressure of 70 bar) could be catalyzed by ^{Cy}**FeH** at 80°C in the presence of 300 equiv. DBU, which yielded formate with a TON of 186 in 12 h [101]. Adding 150 equiv. $LiBF_4$ to the reaction mixture improves the TON to 289 in 4 h. Detailed mechanistic studies by Hazari and Bernskoetter suggest that the Lewis acid disrupts the intramolecular hydrogen bonding interaction between the NH moiety and the formato group and facilitates the release of HCO_2^- from iron [115]. Further screening of Lewis acids reveals that the hydrogenation reaction is best carried out in the presence of LiOTf with an optimal DBU to LiOTf ratio of 7.5 to 1. Under such conditions, hydrogenation of CO_2 catalyzed by ^{iPr}**FeH** and ^{Cy}**FeH** gives formate with TONs of 6,030 and 8,910, respectively (Scheme 19). The borohydride complex

Scheme 19 Hydrogenation of CO_2 to formate catalyzed by various iron-based PNP pincer complexes

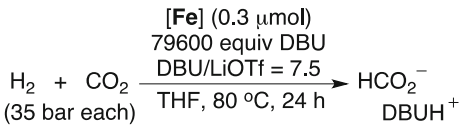

[Fe]	TON
$^{i\mathrm{Pr}}$FeH	6030
$^{\mathrm{Cy}}$FeH	8910
$^{i\mathrm{Pr}}$FeHBH$_4$	1500
($^{i\mathrm{Pr}}$PN$^{\mathrm{Me}}$P)FeH(CO)BH$_4$	42350
($^{\mathrm{Cy}}$PN$^{\mathrm{Me}}$P)FeH(CO)BH$_4$	46110
$^{i\mathrm{Pr}}$FeH(CNAr$^{\mathrm{Me2}}$)	613
$^{i\mathrm{Pr}}$FeH(CNAr$^{\mathrm{OMe}}$)	333
($^{i\mathrm{Pr}}$PN$^{\mathrm{Me}}$P)FeH(CNAr)BH$_4$	5300
($^{i\mathrm{Pr}}$PN$^{\mathrm{Me}}$P)FeH(CN^{t}Bu)BH$_4$	1300
($^{i\mathrm{Pr}}$PN$^{\mathrm{Me}}$P)FeH(CNAd)BH$_4$	710

(Ar = 2,6-dimethylphenyl)

$^{i\mathrm{Pr}}$FeHBH$_4$ displays a lower catalytic activity. Similar to the ruthenium-based catalytic systems, iron-catalyzed hydrogenation of CO_2 to the formate stage does not require the presence of the NH moiety. As a matter of fact, ($^{i\mathrm{Pr}}$PN$^{\mathrm{Me}}$P)FeH(CO)BH$_4$ and ($^{\mathrm{Cy}}$PN$^{\mathrm{Me}}$P)FeH(CO)BH$_4$ are significantly more active with an about 30-fold increase in formate yield. For additional modification to the catalyst structure, Hazari and Bernskoetter incorporated different isocyanide ligands into the PNP pincer system. The five-coordinate complexes **$^{i\mathrm{Pr}}$FeH(CNAr$^{\mathrm{Me2}}$)** and **$^{i\mathrm{Pr}}$FeH(CNAr$^{\mathrm{OMe}}$)** prove to be less active than the CO analog **$^{i\mathrm{Pr}}$FeH** [102]. The second-generation isocyanide-based catalysts supported by the methylated PNP ligand $^{i\mathrm{Pr}}$PN$^{\mathrm{Me}}$P show some improvement over **$^{i\mathrm{Pr}}$FeH(CNAr$^{\mathrm{Me2}}$)** and **$^{i\mathrm{Pr}}$FeH(CNAr$^{\mathrm{OMe}}$)**; however, they are still less effective than the corresponding CO derivatives [116].

Another formally two-electron reduction process with CO_2 is *N*-formylation of amines, as mentioned in the ruthenium systems (Scheme 12). For iron-based catalysts, Bernskoetter compared the activity of **$^{i\mathrm{Pr}}$FeH**, its adduct with HCONHPh, ($^{i\mathrm{Pr}}$PN$^{\mathrm{Me}}$P)FeH(CO)BH$_4$, and *trans*-($^{i\mathrm{Pr}}$PN$^{\mathrm{Me}}$P)FeH$_2$(CO) for the *N*-formylation of morpholine [117]. Under the conditions outlined in Eq. 31, the reaction catalyzed by **$^{i\mathrm{Pr}}$FeH** generates the formamide with a TON of 1930. The catalytic performance is slightly better than the HCONHPh adduct but worse than the methylated PNP complexes, again illustrating that the NH moiety is not needed for CO_2 reduction to the formate stage.

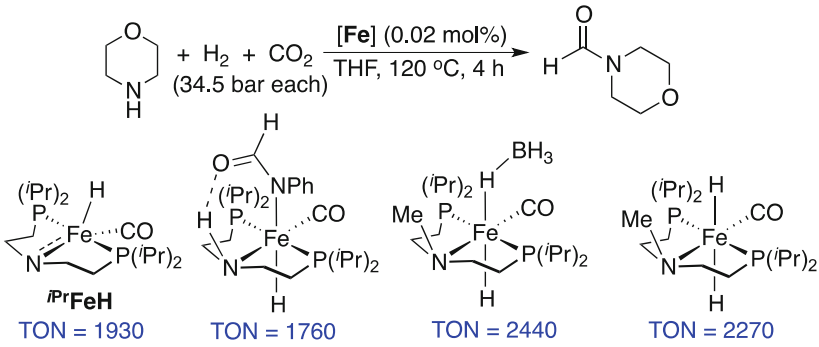

(31)

The iron-catalyzed amide hydrogenation has already been described in the previous section (see Eq. 27). Hydrogenation of formamides to methanol is singled out and discussed here due to its relevance to CO_2 reduction (which changes the carbon oxidation state from +2 to −2). Under Sanford's conditions (0.33 mol% ^{Cy}**FeHBH$_4$**, 1.66 mol% K_3PO_4, 20 bar H_2, 110°C, 3 h), *N*-formylmorpholine, HCONHAr, and $HCONPh_2$ are hydrogenated to methanol with TONs of up to 300 [97]. Hydrogenation of HCONHMe and $HCONH_2$ is problematic, providing methanol with only 1–12% yield. Bernskoetter's system (0.018 or 0.07 mol% ^{iPr}**FeH**, 30.4 bar H_2, 100°C, 4 h) hydrogenates *N*-formylmorpholine, HCONHAr, and $HCONPh_2$ to methanol with TONs typically falling in the range of 1,190–4,430 [110]. Hydrogenation of HCONMePh under the same conditions is low yielding (TON = 60) but can be improved by adding 20 equiv. of HCONHPh (TON = 1,300). The overall hydrogenation process consumes 2 equiv. of H_2 (for a formally four-electron reduction process), first converting formamides to hemiaminals and then to methanol. This requires decomposition of hemiaminals to formaldehyde and amines, a process that can be catalyzed by iron or the formamide substrates, depending on the nitrogen substituents [118].

The process of CO to ethylene glycol via oxamide described in Scheme 13 has also been studied with iron-based PNP pincer complexes (i.e., ^{iPr}**FeHBH$_4$**, ^{Cy}**FeHBH$_4$**, ^{Et}**FeHBH$_4$**, and *trans*-(^{Et}PN^{H}P)$FeBr_2$(CO)), although the focus is on the second step that hydrogenates the oxamide to ethylene glycol [85]. With 0.2 mol % an iron catalyst and 1–1.5 mol% KO^{t}Bu, after 6 h, only 18–53% of the oxamide is hydrogenated. However, using 2 mol% ^{Et}**FeHBH$_4$** along with 5 mol% KOH and extending the reaction time to 24 h leads to a full conversion of the oxamide with 77% of the hydrogenation products attributed to ethylene glycol (Eq. 32).

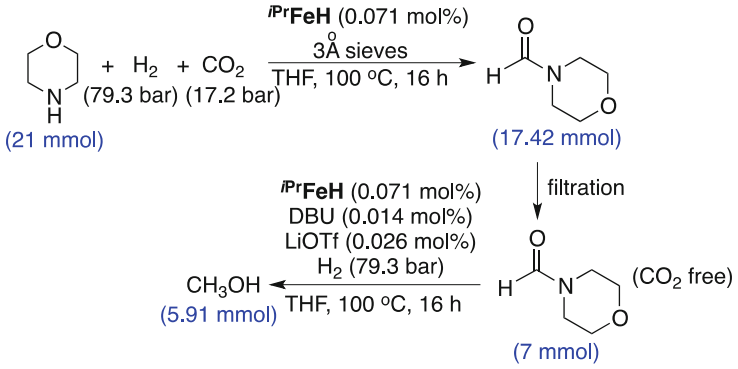

Scheme 20 A two-step hydrogenation of CO_2 to methanol catalyzed by an iron complex

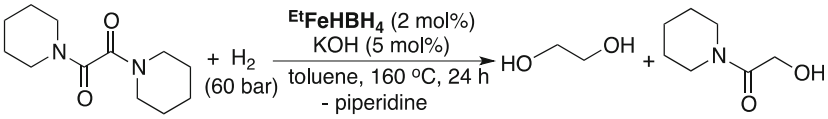

(32)

Direct hydrogenation of CO_2 to methanol assisted by amines, which changes the carbon oxidation state from +4 to −2, is more challenging with iron catalysts due to their relatively low thermal stability. The ruthenium systems described earlier operate most efficiently at 140–160°C. A thermal stability study of **^{iPr}FeHBH$_4$** conducted by Jones showed that at 140°C this compound decomposed completely in 4 h [100]. Nevertheless, some of the iron-based PNP pincer complexes have been tested for this transformation. Olah and Prakash's strategy of using PEHA to capture CO_2 and **^{iPr}FeHBr** to hydrogenate the captured CO_2 (145°C, 70 bar H_2, 72 h) failed to produce any methanol. Instead, formate and formamide were detected with NMR yields of 20% and 18%, respectively [89]. On the other hand, hydrogenation of the captured CO_2 in a biphasic mixture (as illustrated in Scheme 15) was successful with **^{iPr}FeHBr** at 55°C under 50 bar H_2, which, after 10 h, gave formate in 96% yield. Like the **Ru-MACHO-BH** system, the iron catalyst can be reused at least four times without losing the catalytic activity [88].

Given the results in Eq. 31 and the fact that **^{Cy}FeHBH$_4$** and **^{iPr}FeH** catalyze the hydrogenation of formamides to methanol [97, 110], one might expect some catalytic activity from these iron complexes for CO_2 hydrogenation to methanol assisted by amines. A recent study by Bernskoetter suggests that these two steps are incompatible, thus preventing them being carried out in a single reactor [119]. In particular, CO_2 poisons the catalyst during formamide hydrogenation. Furthermore, water (generated from CO_2 hydrogenation) deactivates the catalytically active species. To solve these issues, *N*-formylation of morpholine was first catalyzed by **^{iPr}FeH** in the presence of 3 Å sieves (Scheme 20). The resulting mixture was filtered to remove the sieves as well as ammonium carbamate salt of morpholine. A portion

of the filtered mixture was then subjected to the second hydrogenation step catalyzed by ^{iPr}**FeH**. This two-step procedure provides methanol with a net TON of 590.

3.3 Osmium Catalysts

Osmium complexes have been rarely explored for hydrogenation reactions. DFT calculations on *trans*-(^{iPr}PN^{H}P)MH$_2$(CO) (M = Fe, Ru, Os) suggest that hydrogenation of MeCN is best catalyzed by iron and ruthenium and hydrogenation of methyl benzoate is best catalyzed by ruthenium [120]. Such predications have not been validated experimentally. The only known osmium system involving the PNP-type ligand is the one developed by Gusev, who treated the ^{iPr}PN^{H}P ligand with OsHCl(CO)(PPh$_3$)$_3$ much like for the synthesis of ^{iPr}**RuHCl** (Scheme 21) [57]. The isolated product ^{iPr}**OsHCl** was identified as an isomeric mixture, which underwent dehydrochlorination with KO^{t}Bu followed by dehydrogenation of ^{i}PrOH to yield the dihydride complex ^{iPr}**OsH$_2$**. What is remarkable about these osmium hydride complexes is that both ^{iPr}**OsHCl** and ^{iPr}**OsH$_2$** are air and moisture stable in solution.

In terms of hydrogenation reactions, ^{iPr}**OsHCl** and ^{iPr}**OsH$_2$** have been evaluated to catalyze the hydrogenation of hexyl octanoate, *cis*-3-hexenyl hexanoate, and triglycerides [121]. As for the analogous ruthenium and iron complexes, ^{iPr}**OsHCl** needs to be activated by a strong base such as NaO^{t}Bu. The best conditions for hydrogenating hexyl octanoate (in toluene) involve 0.1 mol% ^{iPr}**OsH$_2$** (loaded in air) at 220°C under 55.2 bar H_2 for 24 h, which results in 87% conversion of the ester with high selectivity for the alcohol products. The mixture of ^{iPr}**OsHCl** and NaO^{t}Bu shows slightly lower activity. The hydrogenation reaction is operative under neat conditions, and loading the catalysts under an inert atmosphere improves the yield by 6–15%. Hydrogenation of *cis*-3-hexenyl hexanoate with the osmium catalysts saturates the C=C bond first, during which process the catalysts also degrade, showing no activity toward the ester functionality. To circumvent the issue, hydrogenation of *cis*-3-hexenyl hexanoate and seed oil (a mixture of canola and soybean oil) is first performed with Pd/C, a heterogeneous catalyst, to saturate the C=C bonds (Scheme 22). After filtration to remove Pd/C, the resulting saturated esters are subjected to hydrogenation catalyzed by ^{iPr}**OsH$_2$**, which reduces the esters with a 60–90% conversion.

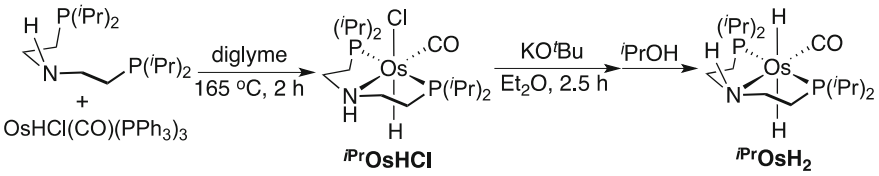

Scheme 21 Synthesis of osmium-based hydrogenation (pre)catalysts

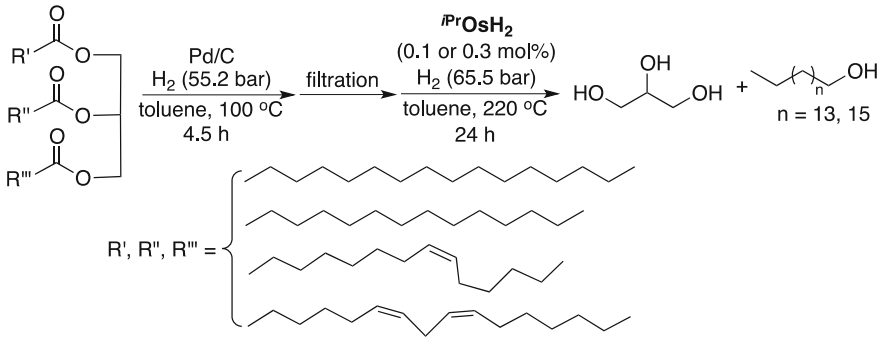

Scheme 22 A two-step process for the hydrogenation of seed oil

4 Group 9 Metal Systems

4.1 Rhodium Catalysts

As mentioned in Introduction, rhodium holds historical significance in hydrogenation catalysis, particularly for the early efforts to hydrogenate C=C bonds. It is thus somewhat surprising that there is very little development of the PNP-ligated rhodium complexes as catalysts for the modern-day hydrogenation reactions. In 1984, Taqui Khan reported the synthesis of ($^{Ph}PN^{H}P$)RhCl from the reaction of $[RhCl(COE)_2]_2$ (COE = cyclooctene) with $^{Ph}PN^{H}P$ in benzene [122]. In a series of subsequent reports, this specific PNP complex was shown to catalyze the hydrogenation of cyclohexene [122], 1-heptene [123], and 1-pentene [124] at 10–50°C under 0.4–1 bar H_2. The proposed mechanism is analogous to the one for Wilkinson's $RhCl(PPh_3)_3$ catalyst, which involves H_2 activation followed by olefin coordination [125]. Based on the NMR analysis, oxidative addition of H_2 to ($^{Ph}PN^{H}P$)RhCl produces thee dihydride complexes with the formula ($^{Ph}PN^{H}P$)RhH_2Cl. The major product (90%) is consistent with *cis*-($^{Ph}PN^{H}P$)RhH_2Cl with the $^{Ph}PN^{H}P$ ligand adopting the meridional configuration [126]. A more recent study by Jagirdar showed that ($^{Ph}PN^{H}P$)RhH_2Cl was unable to catalyze the hydrogenation of aldehydes, ketones, imines, and CO_2 at 50°C under 20 bar H_2 [127]. These results do not rule out the possibility of using the rhodium-based PNP-type complexes for the hydrogenation of polar bonds, because the hydrogenation reactions were attempted under base-free conditions and the active species could be ($^{Ph}PN^{H}P$)RhH_3.

4.2 Cobalt Catalysts

4.2.1 Synthesis of (Pre)catalysts

In contrast to the limited examples for the PNP-type complexes of rhodium, many cobalt derivatives have been studied, including spectroscopic observation and crystallographic characterization of ($^{i\mathrm{Pr}}$PN$^{\mathrm{H}}$P)CoH_2Cl and ($^{i\mathrm{Pr}}$PN$^{\mathrm{H}}$P)CoH_3 [128]. While these Co(III) hydrides have yet to be employed for hydrogenation reactions, close to a dozen cobalt complexes supported by the $^{\mathrm{R}}$PN$^{\mathrm{H}}$P ligands have been prepared (Scheme 23) and evaluated as hydrogenation catalysts.

As illustrated in Scheme 23, the first class of cobalt PNP-type complexes feature an alkyl or aryl donor, and the synthesis starts with $(pyr)_2Co(CH_2SiMe_3)_2$ (pyr = pyridine) (Method A). Its ligand substitution reaction with $^{\mathrm{Cy}}$PN$^{\mathrm{H}}$P gives **$^{\mathrm{Cy}}$CoCH$_2$TMS**, which can be protonated on the nitrogen by Brookhart's acid, $[H(OEt_2)_2]BAr^F{}_4$, to form a cationic complex **[$^{\mathrm{Cy}}$CoCH$_2$TMS]$^+$** [16]. Treatment of **[$^{\mathrm{Cy}}$CoCH$_2$TMS]$^+$** with 1-phenylethanol results in a Co(III) hydride **[$^{\mathrm{Cy}}$CoHAr]$^+$**, which appears to dehydrogenate the alcohol and then activate the C–H bond of the dehydrogenation product, acetophenone [129].

The reaction of a $^{\mathrm{R}}$PN$^{\mathrm{H}}$P ligand with $CoCl_2$ or $CoBr_2$ provides another entry to cobalt-based PNP-type complexes (Method B). Exposure of **$^{i\mathrm{Pr}}$CoCl$_2$** and **$^{i\mathrm{Pr}}$CoBr$_2$** to CO produces **$^{i\mathrm{Pr}}$CoCl$_2$(CO)** and **$^{i\mathrm{Pr}}$CoBr$_2$(CO)** [48, 49, 52], and reduction of

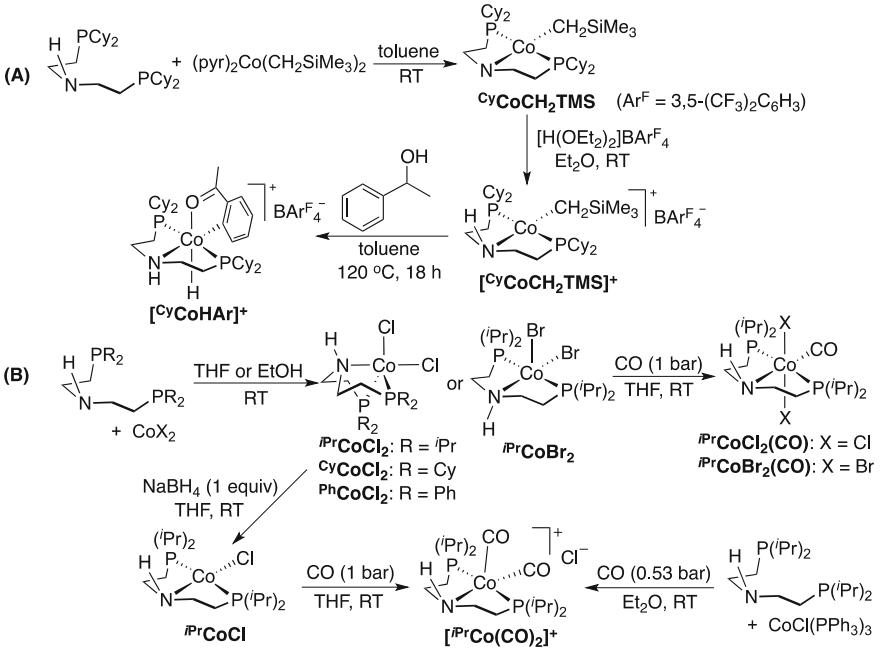

Scheme 23 Synthetic routes to cobalt-based hydrogenation (pre)catalysts

^{iPr}CoCl$_2$ with 1 equiv. of $NaBH_4$ generates a Co(I) species **^{iPr}CoCl** [48]. The latter compound can react with CO to yield a cationic bis(carbonyl) complex **[^{iPr}Co(CO)$_2$]$^+$** [48], which can alternatively be prepared from the reaction of ^{iPr}PN^{H}P with $CoCl(PPh_3)_3$ under CO [130].

4.2.2 Applications for Catalytic Hydrogenation Reactions

The first hydrogenation system involving the cobalt-based PNP-type complexes appeared in a 2012 report by Hanson [16]. In that study, 1:1 mixture of **^{Cy}CoCH$_2$TMS** and $[H(OEt_2)_2]BAr^F{}_4$, which essentially generated **[^{Cy}CoCH$_2$TMS]$^+$** in situ, was shown to catalyze the hydrogenation of terminal and disubstituted (1,1- or 1,2-) olefins at 25°C under an atmospheric H_2 pressure (Eq. 33). Without the acid, **^{Cy}CoCH$_2$TMS** alone is almost completely inactive. Aldehydes, ketones, and aldimines are also viable substrates under same conditions or a slightly higher temperature and/or H_2 pressure. At 25°C, hydrogenation of C=C bonds is unaffected by the presence of an ester, carboxylic acid, amine, or alcohol group in the olefin substrate and only slightly inhibited by water.

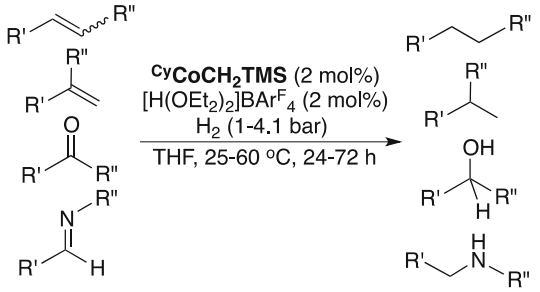

(33)

In a follow-up study, Hanson used the methylated PNP complex [(^{Cy}PN^{Me}P)$CoCH_2SiMe_3$]$BAr^F{}_4$ to probe the role that NH moiety could play during the hydrogenation reactions [129]. Evidently, the NH functionality is not needed for olefin hydrogenation but absolutely required for ketone hydrogenation (performed at 25–60°C under 1 bar H_2). The lack of metal-ligand cooperation in olefin hydrogenation has been supported by DFT calculations [131]. The proposed mechanism involves C=C bond insertion into the Co–H bond of [(^{Cy}PN^{H}P)CoH]$BAr^F{}_4$ or [(^{Cy}PN^{Me}P)CoH]$BAr^F{}_4$ followed by hydrogenolysis of the cobalt alkyl species, in which NH or NMe does not directly participate. The Co(III) hydride **[^{Cy}CoHAr]$^+$** also shows good activity for hydrogenating styrene under ambient conditions but limited activity for hydrogenating acetophenone even at 60°C under 4.1 bar H_2 [129].

Under more forcing conditions, carbonyl groups can be hydrogenated, not only by **[^{Cy}CoCH$_2$TMS]$^+$** but also by the methylated derivative [(^{Cy}PN^{Me}P)$CoCH_2SiMe_3$]$BAr^F{}_4$. Jones reported in 2017 that both cationic complexes were effective catalysts for ester (or lactone) hydrogenation at 120°C under 55 bar H_2

(Eq. 34) [132]. As expected, hydrogenation of α,β-unsaturated esters with **[^{Cy}CoCH$_2$TMS]$^+$** results in both C=C and C=O bonds being reduced, although C=C bond hydrogenation appears to be faster. In contrast to olefin hydrogenation described earlier, carboxylic acid interferes with ester hydrogenation. No hydrogenation product was observed when adipic acid monoethyl ester was employed as the substrate. The uniqueness about this cobalt-based catalytic system is that methyl esters usually give lower alcohol yields when compared to the corresponding ethyl esters. Mechanistic investigation focusing on methyl benzoate revealed that **[^{Cy}CoCH$_2$TMS]$^+$** lost its catalytic activity by forming [(^{Cy}PN^{H}P)Co(κ^1-OCOPh)(κ^2-OCOPh)]BAr$^F{}_4$, presumably via methane elimination. Similar to the mechanism proposed for olefin hydrogenation, [(^{Cy}PN^{H}P)CoH]BAr$^F{}_4$ or [(^{Cy}PN^{Me}P)CoH]BAr$^F{}_4$ is thought to be the active species, although according to DFT calculations, some of intermediates during ester hydrogenation feature a significant distortion of the PNP ligand from the meridional geometry [133].

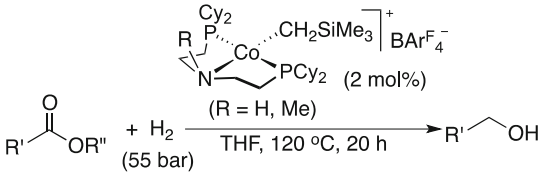

(34)

Under similar conditions (100–140°C, 50 bar H_2), the cobalt complexes listed in Scheme 23, Method B, when activated by NaOMe, all display some level of catalytic activity for the hydrogenation of methyl benzoate [48]. The best precatalyst is **^{Ph}CoCl$_2$**, which promotes the hydrogenation of various esters including lactones (Eq. 35). Unlike the catalytic system shown in Eq. 34, here C=C bonds can be tolerated. Substrates that lead to low alcohol yields include PhCO$_2{}^t$Bu (due to sterics) and chloro- or bromo-substituted methyl benzoate (due to dehalogenation). This particular catalytic system proves to operate via metal-ligand cooperation; control experiments using the methylated complex (^{Ph}PN^{Me}P)CoCl$_2$ did not yield any hydrogenation products.

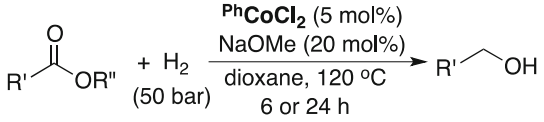

(35)

The cobalt-based PNP-type complexes can also be used to catalyze the hydrogenation of other multiple bonds including those in nitriles and *N*-heterocycles. In 2018, we reported that catalytic hydrogenation of PhCN could be affected by **^{iPr}CoCl$_2$** or **^{iPr}CoBr$_2$** in the presence of NaHBEt$_3$, forming PhCH=NCH$_2$Ph exclusively as the hydrogenation product (Scheme 24) [134]. Adding 1 equiv. of CyNH$_2$ to the reaction generated PhCH=NCy selectively, which represents a hydrogenative coupling process. The selectivity of nitrile hydrogenation can be altered to favor primary amines, as demonstrated by Beller in a more recent study [135]. Among the

Scheme 24 Cobalt-catalyzed hydrogenation of nitriles leading to secondary imines or primary amines

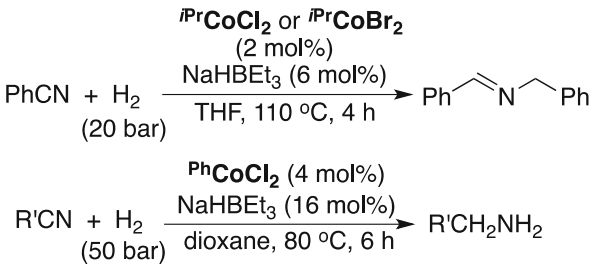

PNP-ligated cobalt dihalide complexes shown in Scheme 23, **^{Ph}CoCl$_2$** is the most active precatalyst, converting various aromatic and aliphatic nitriles to primary amines (Scheme 24). Functional groups tolerated under the catalytic conditions include F, Cl, NH_2, OMe, pyridyl, and pyrrolidyl groups; however, carbonyl groups in esters, ketones, and aldehydes are also hydrogenated along with the nitrile groups. The nature of the catalytically active species is ill-defined here, although all experiments suggest that the hydrogenation process is homogeneous. The lack of reactivity with the methylated complex (^{Ph}PN^{Me}P)CoCl$_2$ also supports a metal-ligand cooperative mechanism.

As a further exploration of *N*-heterocycles as organic hydrogen storage materials, Jones studied the ability of **[^{Cy}CoCH$_2$TMS]$^+$** to catalyze the hydrogenation of these molecules [136]. Under the conditions shown in Eq. 36, the hydrogenation process takes place very slowly, accepting 2 equiv. of H_2 to saturate one nitrogen-containing ring. In contrast to the iron-based catalytic system (Eq. 29), 2,6-lutidine is not a viable substrate for the cobalt catalyst. Analogous to the olefin hydrogenation catalyzed by **[^{Cy}CoCH$_2$TMS]$^+$**, the NH moiety is not needed here.

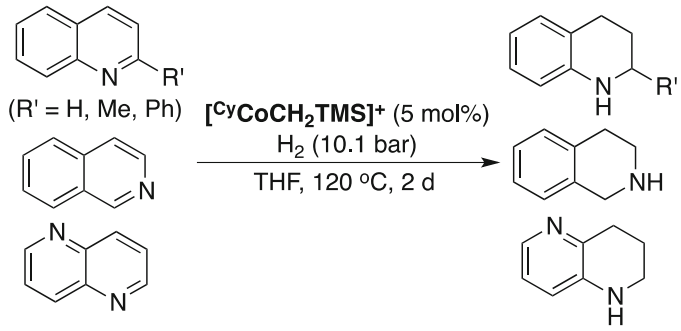

(36)

Catalytic hydrogenation of CO_2 has not been explored extensively with the cobalt-based PNP-type complexes described above. The only known example is Bernskoetter's study of **[^{iPr}Co(CO)$_2$]$^+$** as a potential catalyst [130]. Under the conditions outlined in Eq. 37, hydrogenation of CO_2 gives the formate with 450 turnovers. Similar to the iron-based system (Scheme 19), the methylated complexes [(^{iPr}PN^{Me}P)Co(CO)$_2$]Cl and [(^{Cy}PN^{Me}P)Co(CO)$_2$]Cl are more superior catalysts than **[^{iPr}Co(CO)$_2$]$^+$** for CO_2 hydrogenation, increasing the TON by 64- or 53-fold

[137]. Once again, for CO_2 hydrogenation of to the formate stage, the metal-ligand bifunctional catalysts do not appear to have any advantage.

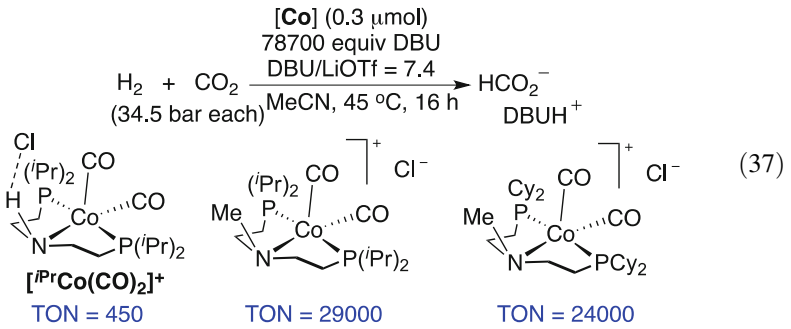

(37)

4.3 Iridium Catalysts

4.3.1 Synthesis of (Pre)catalysts

Iridium-based PNP-type complexes are also known in the literature. To develop a hydrogenation catalyst, Taqui Khan treated $[Ir(COE)_2Cl]_2$ with the hydrochloride salt of $^{Ph}PN^{H}P$ in refluxing benzene, which resulted in a compound with the formula $(^{Ph}PN^{H}P)IrCl$, presumably **^{Ph}IrCl** as shown in Scheme 25 [122]. A more recent synthesis by Jagirdar employed $[Ir(COD)Cl]_2$ and the neutral ligand $^{Ph}PN^{H}P$, which formed $[(^{Ph}PN^{H}P)Ir(COD)]Cl$ with the COD ligand still bound to iridium [127]. Subsequent hydrogenation produced an air-stable Ir(III) dihydride **^{Ph}IrH$_2$Cl**, which was further converted to **^{Ph}IrH$_3$** via dehydrochlorination under H_2. It is interesting to

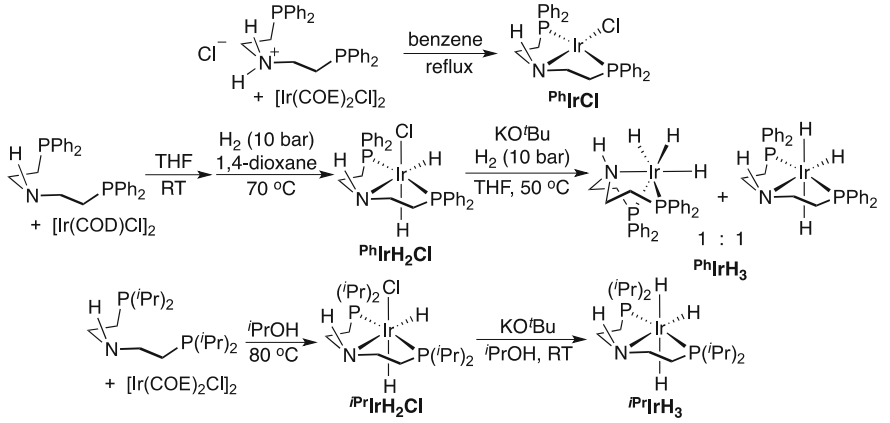

Scheme 25 Synthesis of iridium-based hydrogenation (pre)catalysts

note that **^{Ph}IrH$_3$** exists as a 1:1 isomeric mixture with the PNP ligand adopting either meridional or facial coordination mode. In contrast, the isopropyl analog **^{iPr}IrH$_3$** displays the meridional mode only. This trihydride complex can be prepared from dehydrochlorination of the dihydride **^{iPr}IrH$_2$Cl** followed by dehydrogenation of ^{i}PrOH [138]. **^{iPr}IrH$_2$Cl** is commercially available but can be made from ^{iPr}PN^{H}P and $[Ir(COE)_2Cl]_2$ in ^{i}PrOH at 80°C. It is also worth to point out that in the solid form **^{iPr}IrH$_2$Cl** is air stable and **^{iPr}IrH$_3$** is moderately air stable.

4.3.2 Applications for Catalytic Hydrogenation Reactions

The use of iridium-based PNP-type complexes for catalytic hydrogenations reactions can be traced back to 1984, when Taqui Khan studied the hydrogenation of cyclohexene catalyzed by **^{Ph}IrCl** [122]. This reaction operates over the temperature range 20–50°C under 0.4–1 bar H_2 and proceeds via an initial H_2 activation to form **^{Ph}IrH$_2$Cl** [125]. The catalytic system that really takes advantage of metal-ligand cooperativity is the one developed by Abdur-Rashid in 2009 [139]. It was reported that aldehyde and ketone hydrogenation could be catalyzed by **^{iPr}IrH$_2$Cl** activated with KO^{t}Bu or by **^{iPr}IrH$_3$** under base-free conditions. The catalysts are remarkably active at room temperature; the TONs for acetophenone hydrogenation are as high as 30,000 (Eq. 38). Hydrogenation of benzalacetone and β-ionone is chemoselective for the C=O bonds; however, hydrogenation of 2-cyclohexen-1-one produces a 1:1 mixture of allyl alcohol and the fully saturated alcohol. In a related study, Jagirdar examined the catalytic activity of the phenyl derivatives (**^{Ph}IrH$_3$** and **^{Ph}IrH$_2$Cl**/KO^{t}Bu) in hydrogenation reactions, which were carried out at 50°C in methanol under 20 bar H_2 with a catalyst loading of 0.1 mol% [127]. In addition to aldehydes and ketones, imines such as PhCH=NPh and PhCH=NBn are hydrogenated, albeit with moderate conversions (31–49% over 6 h). In contrast, methyl benzoate and styrene are completely unreactive.

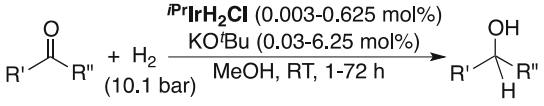

(38)

Abdur-Rashid's iridium complex **^{iPr}IrH$_2$Cl** has also been utilized to catalyze the hydrogenation of alkyl levulinates to γ-valerolactone (Eq. 39) [71]. The reaction is enhanced by added ethanol or methanol, and under the optimized conditions, γ-valerolactone was obtained with TONs of up to 9,300. Compared to **Ru-MACHO**, **^{iPr}IrH$_2$Cl** is more active, although the ruthenium catalyst can be reused three times without noticeable catalyst decomposition.

Scheme 26 Iridium-catalyzed hydrogenation of CO_2 or *N*-formylation of morpholine

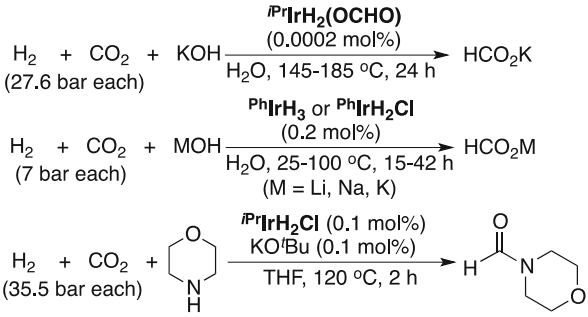

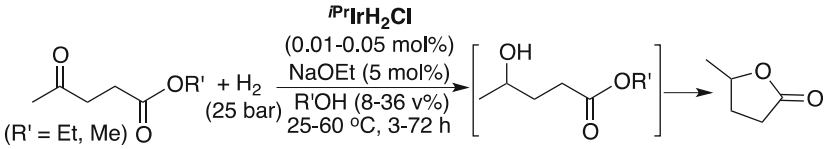

(39)

Esters can be hydrogenated with the iridium-based PNP-type complexes, although the reaction must be conducted at higher temperatures and under higher H_2 pressures. In 2014, Beller showed that in the presence of NaOMe and at 130°C under 50 bar H_2, both ^{iPr}**IrH$_2$Cl** and ^{iPr}**IrH$_3$** were efficient for catalytic hydrogenation of methyl benzoate [140]. Based on the proposed mechanism, ^{iPr}**IrH$_3$** is the active species transferring H^+/H^- to the ester substrate, and therefore the base should not be needed for ^{iPr}**IrH$_3$**. However, the addition of NaOMe does improve the conversion and yield, suggesting that the base plays multiple roles during the reaction. The catalytic system (Eq. 40) can tolerate functional groups including halogens, MeO, pyridyl, and furyl groups. Hydrogenation of *p*-$NCC_6H_4CO_2Me$ and $PhCH{=}CHCO_2Me$ leads to saturation of C≡N, C=O, and C=C bonds. Hydrogenation of phthalic anhydride, on the other hand, can stop at the lactone stage to give phthalide in 71% yield.

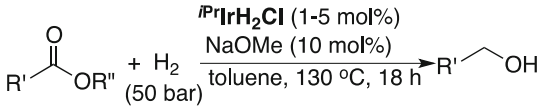

(40)

Another important type of carbonyl substrates for the iridium-catalyzed hydrogenation reactions is CO_2. In 2011, Hazari reported a very facile CO_2 insertion process with ^{iPr}**IrH$_3$**, resulting in an iridium formate complex ^{iPr}**IrH$_2$(OCHO)** that is air stable and features a hydrogen bond between the NH group and the formato group (Eq. 41) [141]. ^{iPr}**IrH$_2$(OCHO)** was then employed to catalyze the hydrogenation of CO_2 in an aqueous solution of KOH (1 M), providing HCO_2K with TONs of up to 348,000 (Scheme 26). The trihydride ^{iPr}**IrH$_3$** can also be used as the catalyst, although precaution needs to be taken to exclude oxygen from the reactor. Very recently, Jagirdar demonstrated that the phenyl derivative ^{Ph}**IrH$_3$** (a 1:1

isomeric mixture) reacted with CO_2 (1 bar at room temperature) to form an insertion product analogous to **^{iPr}IrH$_2$(OCHO)** [127]. Hydrogenation of CO_2 in MOH (M = Li, Na, K) with **^{Ph}IrH$_3$** or **^{Ph}IrH$_2$Cl** produced HCO_2M with much lower TONs of 65–144, although the hydrogenation reactions were tested under relatively low temperatures and pressures. In studying *N*-formylation of morpholine, Ding also examined the catalytic activity of **^{iPr}IrH$_2$Cl** (activated by KO^{t}Bu), which, under the conditions shown in Scheme 26, generated the formamide with a TON of 720 [82]. An attempt to use ethylene carbonate as CO_2 surrogate had limited success with **^{iPr}IrH$_2$Cl**/KO^{t}Bu as the catalyst (0.1 mol%); at 140°C under 50.7 bar H_2, ethylene glycol was obtained with only 10% yield [55]. The ruthenium system shown in Eq. 23 is far more reactive.

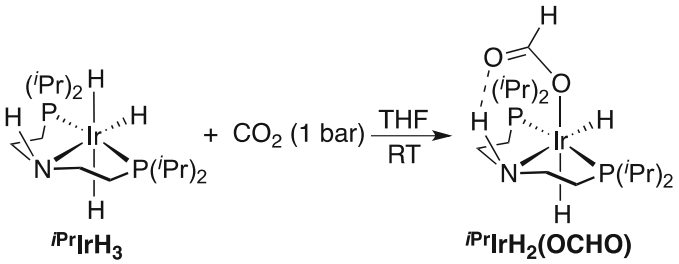

(41)

5 Group 10 Metal Systems

Group 10 metals bearing the PNP-type ligands have been rarely used as hydrogenation catalysts. The only known example of a nickel system is the one developed by Hanson in 2012 [142]. As summarized in Scheme 27, the reaction of Ni(diglyme)Br_2 with $^{Cy}PN^HP$ produces a cationic PNP pincer nickel bromide complex, which can be converted to the hydride **[^{Cy}NiH]$^+$** using $NaBH_4$ followed by anion exchange with $NaBPh_4$. The neutral hydride **^{Cy}NiH** is available from **[^{Cy}NiH]$^+$** through deprotonation with KH.

Complex **[^{Cy}NiH]$^+$** proves to be an active catalyst for the hydrogenation of styrene, α-methylstyrene, and *tert*-butylethylene at 80°C under 4.1 bar H_2 (Eq. 42) [142]. Hydrogenation of 1-octene affords *n*-octane and internal octenes as a result of the competing olefin isomerization process. Under similar conditions, aldehydes are reduced to alcohols but in a non-catalytic manner. The neutral hydride **^{Cy}NiH** is also

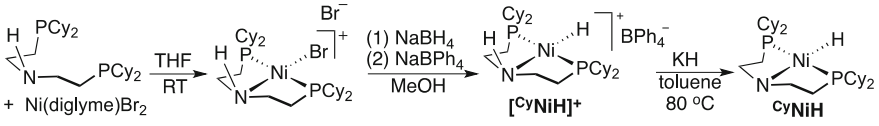

Scheme 27 Synthesis of PNP-ligated nickel hydride complexes

an active catalyst, although it is less reactive than **[^{Cy}NiH]$^+$**. The methylated complex (^{Cy}PN^{Me}P)NiH]BPh$_4$ shows similar activity to **[^{Cy}NiH]$^+$**, suggesting that here a metal-ligand cooperative mechanism is not involved.

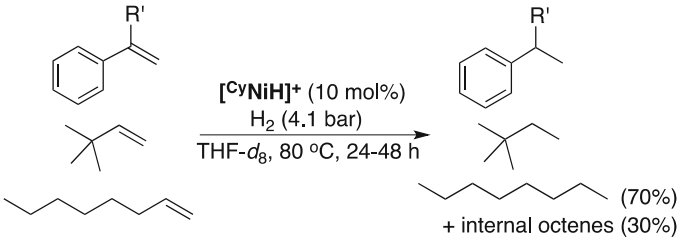

(42)

The analogous palladium and platinum hydrides have not been reported in the literature. The most relevant study is a 1988 report by Taqui Khan, who used [(^{Ph}PN^{H}P)PdCl]Cl (made from Pd(COD)Cl$_2$ and the hydrochloride salt of ^{Ph}PN^{H}P in benzene) to catalyze hydrogenation of cyclohexene [143]. The reaction was shown to operate at 10–40°C under 0.4–1 bar H_2 and proceed via a palladium hydride intermediate.

6 Group 6 Metal Systems

Mid-transition metal complexes supported by the PNP-type ligands have been studied. For group 6 metal systems, chromium complexes have never been utilized to catalyze hydrogenation reactions, although (^{R}PN^{H}P)CrCl$_2$ [144] and (^{R}PN^{H}P)CrCl$_3$ [145] have been known for many years. In contrast, PNP-ligated molybdenum and tungsten complexes have been developed specifically for various hydrogenation processes. They belong to two different types of complexes, each with a d^6 electron configuration and isoelectronic to (^{R}PNP)Fe(CO)H, which have already been established as active hydrogenation catalysts.

6.1 Nitrosyl Complexes

To synthesize the desired nitrosyl complexes (^{R}PNP)M(NO)CO (M = Mo, W), Berke used M(NO)(CO)$_4$(AlCl$_4$) as the metal precursors, which were shown to react with the ^{iPr}PN^{H}P ligand to form (^{iPr}PN^{H}P)M(NO)(CO)Cl (Scheme 28) [146]. Upon further treatment with NaN(SiMe$_3$)$_2$, the five-coordinate complexes **^{iPr}MoNO** and **^{iPr}WNO** were isolated as highly air-sensitive materials.

Activation of H_2 by **^{iPr}MoNO** and **^{iPr}WNO** is feasible but slow at room temperature, forming a mixture of two isomers because of the availability of two sides (NO side vs. CO side) for H_2 to approach (Eq. 43). As expected for other H–M–N–

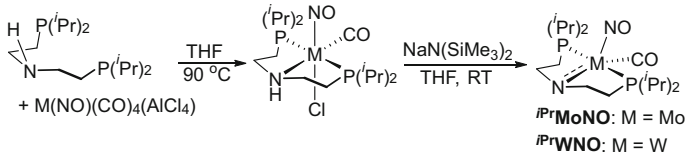

Scheme 28 Synthesis of Mo- and W-based hydrogenation catalysts bearing a nitrosyl ligand

Scheme 29 Molybdenum- and tungsten-catalyzed hydrogenation of imines and nitriles

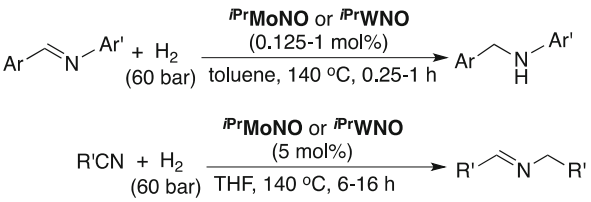

H-type complexes, reduction of polar bonds is likely to occur with these hydrides. Indeed, Berke demonstrated that **$^{i\mathrm{Pr}}$MoNO** and **$^{i\mathrm{Pr}}$WNO** were efficient catalysts for the hydrogenation of aldimines bearing various aryl substituents (Scheme 29) [146]. Substrates that are unreactive under the catalytic conditions include *p*-$NO_2C_6H_4CH{=}NPh$, $PhCH{=}N^iBu$, and surprisingly PhCHO. Acetophenone can be hydrogenated but with a low yield of 32%. Under slightly modified conditions, both aliphatic and aromatic nitriles are hydrogenated with selectivity favoring the secondary imines [147]. This implies that hydrogenation of the intermediate $R'CH{=}NH$ to $R'CH_2NH_2$ is less competitive than the reaction of $R'CH{=}NH$ with $R'CH_2NH_2$ to yield $R'CH{=}NCH_2R'$. In both catalytic processes, **$^{i\mathrm{Pr}}$MoNO** displays high activity than **$^{i\mathrm{Pr}}$WNO**, which is also confirmed by DFT calculations [148].

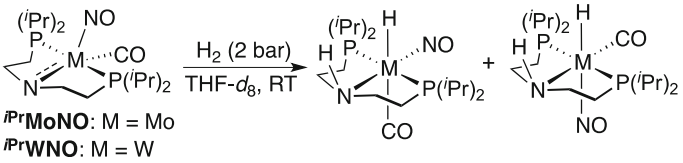

(43)

Attempts have also been made to use **$^{i\mathrm{Pr}}$MoNO** and **$^{i\mathrm{Pr}}$WNO** to catalyze CO_2 hydrogenation [149]. The in situ generated hydrides (see Eq. 43) were shown to undergo CO_2 insertion to generate molybdenum and tungsten formate complexes, which could be converted back to **$^{i\mathrm{Pr}}$MoNO** and **$^{i\mathrm{Pr}}$WNO** through the addition of $NaN(SiMe_3)_2$. Unfortunately, catalytic hydrogenation of CO_2 (p_{H2} = 70 bar, p_{CO2} = 10 bar, 140°C) in the presence of a base and with **$^{i\mathrm{Pr}}$MoNO** or **$^{i\mathrm{Pr}}$WNO** (5 mol%) failed to produce HCO_2^- with a yield greater than 5%. This is likely due to the poisoning of the catalysts by CO_2 to form carbamate species (Eq. 44), as separately studied.

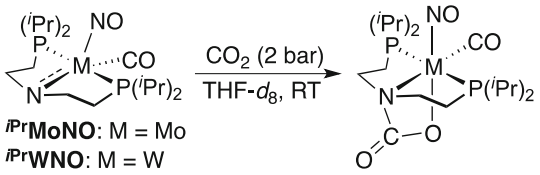

(44)

6.2 Bis(Carbonyl) Complexes

The bis(carbonyl) system illustrated in Fig. 5 has recently been explored, though only focusing on molybdenum complexes. As shown in Scheme 30, treatment of $^{i\mathrm{Pr}}\mathrm{PN^HP}$ with $Mo(CO)_6$ and $Mo(PPh_3)_2(CO)_2(MeCN)_2$ leads to ligand substitution, which generates **$^{i\mathrm{Pr}}$Mo(CO)$_3$** and **$^{i\mathrm{Pr}}$MoNCMe**, respectively [150]. The latter reaction needs to be carried out in THF. Switching the solvent to CH_2Cl_2 can oxidize Mo (0) to Mo(I), giving the chloride complex **$^{i\mathrm{Pr}}$MoCl**. The analogous bromide complex **$^{i\mathrm{Pr}}$MoBr** is isolated as the minor product from the reaction of $^{i\mathrm{Pr}}\mathrm{PN^HP}$ with Mo(η^3-allyl)$(PPh_3)_2(CO)_2(MeCN)_2$Br (the major product is **$^{i\mathrm{Pr}}$MoNCMe**).

Both **$^{i\mathrm{Pr}}$MoCl** and **$^{i\mathrm{Pr}}$MoNCMe**, when activated by $NaHBEt_3$, catalyze the hydrogenation of acetophenone, whereas **$^{i\mathrm{Pr}}$Mo(CO)$_3$** shows no activity [150]. Under the optimized conditions for **$^{i\mathrm{Pr}}$MoCl** (Scheme 31), acetophenones substituted by F, MeO, MeS, and CF_3 groups are all successfully hydrogenated to the corresponding alcohols in high yields. The reaction of (*E*)-PhCOCH=CHPh

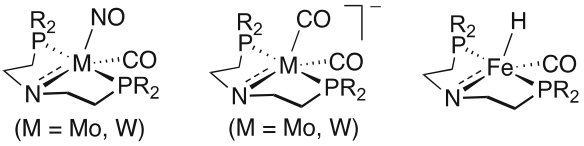

Fig. 5 Molybdenum and tungsten complexes isoelectronic to ($^{\mathrm{R}}$PNP)Fe(CO)H

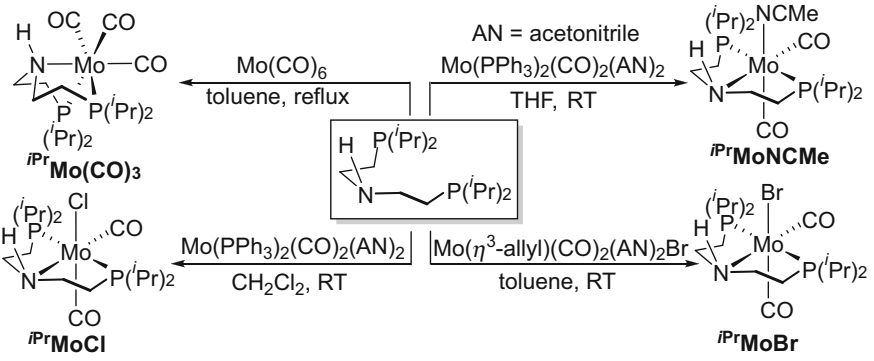

Scheme 30 Synthesis of molybdenum-based precatalysts bearing at least two CO ligands

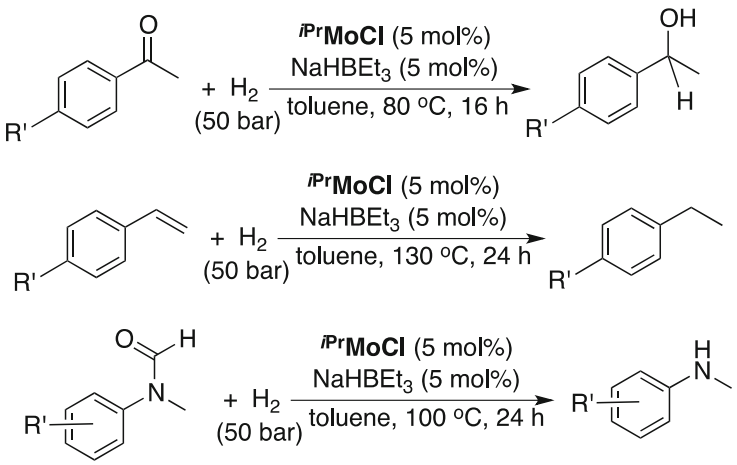

Scheme 31 Hydrogenation reactions catalyzed by ^{iPr}**MoCl**-$NaHBEt_3$

results in both double bonds being reduced. Styrene derivatives are also viable substrates, although a higher temperature of 130°C is required. Hydrogenation reactions performed at 100°C allow the conversion of *N*-methylformanilides to *N*-methylanilines with C=C bond and ester functionality intact [151]. Other functional groups including $PhCH_2O$, Me_2N, CN, and NO_2 are also compatible with the catalytic conditions; however, the product yields are low to moderate (6–52%). Amides of the type R′CONPhR″ (R′ = Me, CF_3, Ph) are more challenging substrates, which typically give 11–28% yields for the hydrogenation products. The bromide complex ^{iPr}**MoBr** shows similar activity to ^{iPr}**MoCl** but outperforms ^{iPr}**MoNCMe**. The ^{iPr}**Mo(CO)$_3$** is completely inactive. A detailed mechanistic study [151] focusing on ^{iPr}**MoCl** suggests that $NaHBEt_3$ reduces the Mo (I) complex to several Mo(0) species including Na[(^{iPr}PN^{H}P)Mo$(CO)_2$H] and Na [(^{iPr}PNP)Mo$(CO)_2$]. These two complexes represent the H–M–N–H and M–N molecules characteristic of metal-ligand bifunctional hydrogenation catalysts.

7 Group 7 Metal Systems

7.1 Manganese Catalysts

There has been an increasing interest in developing manganese-based hydrogenation catalysts [152]. This is in part motivated by the fact that manganese is the third most abundant transition metal (after iron and titanium) in the Earth's crust. For PNP-type complexes, manganese species isoelectronic to (^{R}PNP)Fe(CO)H would be (^{R}PNP) $Mn(CO)_2$. To date, strategies of using inexpensive sources of manganese such as $MnCl_2$ to make these Mn(I) complexes have not had much success. For example,

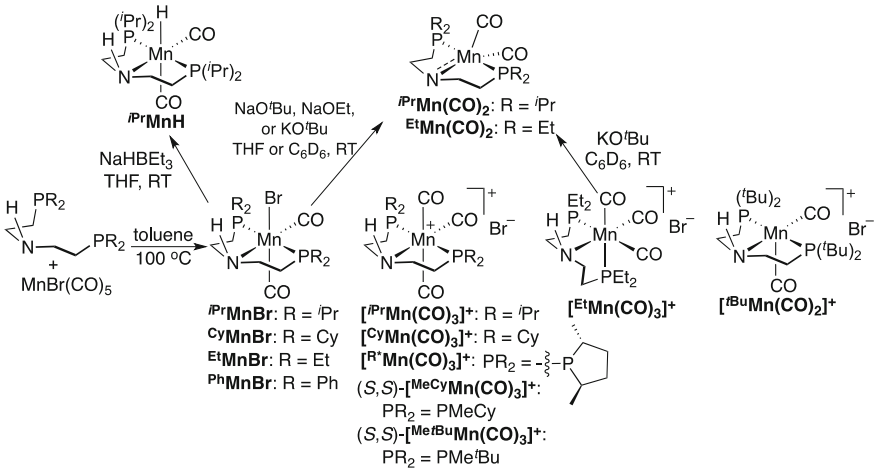

Scheme 32 Synthesis of manganese-based (pre)catalysts

($^{i\text{Pr}}$PN$^{\text{H}}$P)MnCl$_2$ prepared from $^{i\text{Pr}}$PN$^{\text{H}}$P and MnCl$_2$ does not bind CO [153]. Successful routes to the carbonyl complexes have relied on the use of MnBr(CO)$_5$ as the metal precursor. As illustrated in Scheme 32, the reaction of $^{\text{R}}$PN$^{\text{H}}$P with MnBr(CO)$_5$ can lead to four different structures, which depend on the nature of phosphorus substituents. With medium-sized alkyl groups (R = ^{i}Pr, Cy, Et), a mixture of neutral dicarbonyl and cationic tricarbonyl complexes (e.g., **$^{i\text{Pr}}$MnBr** and **[$^{i\text{Pr}}$Mn(CO)$_3$]$^+$**) is obtained [154]. The $^{\text{R}}$PN$^{\text{H}}$P ligands all adopt the meridional coordination mode, except that in **[$^{\text{Et}}$Mn(CO)$_3$]$^+$**, the $^{\text{Et}}$PN$^{\text{H}}$P ligand occupies three facial coordination sites [37]. The dicarbonyl and tricarbonyl complexes are separable due to solubility difference, although higher temperatures and longer reaction times usually facilitate the conversions to the neutral products. The phospholane-based chiral ligand, (*S*,*S*)-(CyMePCH$_2$CH$_2$)$_2$NH, and (*S*,*S*)-(^{t}BuMePCH$_2$CH$_2$)$_2$NH can generate the cationic tricarbonyl complexes only [155, 156], whereas the more bulky ligand $^{t\text{Bu}}$PN$^{\text{H}}$P leads to further extrusion of CO to yield **[$^{t\text{Bu}}$Mn(CO)$_2$]$^+$** [154]. The reaction of the phenyl-substituted ligand $^{\text{Ph}}$PN$^{\text{H}}$P gives the neutral dicarbonyl complex **$^{\text{Ph}}$MnBr** [157]. Synthesis of the five-coordinate complexes **^{i}PrMn(CO)$_2$** and **$^{\text{Et}}$Mn(CO)$_2$** has been accomplished via dehydrobromination of **$^{i\text{Pr}}$MnBr** [154, 158], **$^{\text{Et}}$MnBr** [37], and **[$^{\text{Et}}$Mn(CO)$_3$]$^+$** [37] with a strong base. The hydride **$^{i\text{Pr}}$MnH** is available from the reaction of **$^{i\text{Pr}}$MnBr** with NaHBEt$_3$ [153].

The seminal work by Beller in 2016 showed that in the presence of NaO^{t}Bu, **$^{i\text{Pr}}$MnBr** were efficient in catalyzing the hydrogenation of nitriles, ketones, and aldehydes (Scheme 33) [153]. The relative difficulty for hydrogenating these substrates is reflected by the temperature and H_2 pressure employed. As expected, aldehydes are the easiest ones to react. Various functional groups including halogens, CF_3, NH_2, pyridyl, furyl, and isolated C=C bonds are tolerated under these conditions. The nitrile hydrogenation shows excellent selectivity for primary amines. Hydrogenation of PhCH=CHCN produces the allylic and fully saturated

Scheme 33 Manganese-catalyzed hydrogenation of nitriles, ketones, and aldehydes

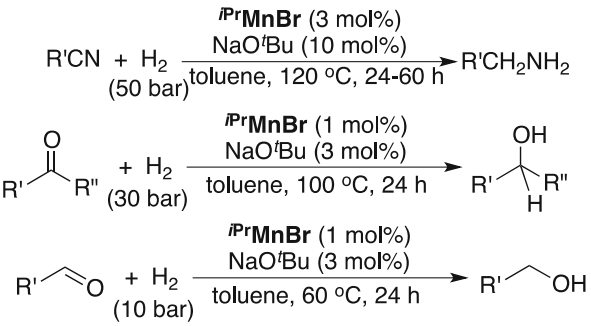

Scheme 34 Manganese-catalyzed asymmetric hydrogenation of ketones

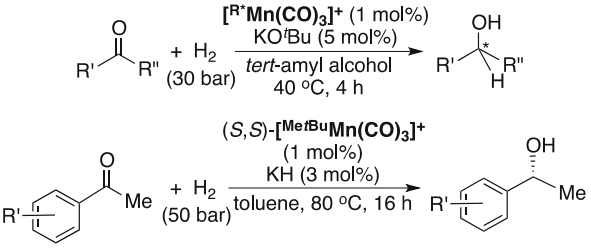

amines. In contrast, hydrogenation of α,β-saturated aldehydes is highly selective for the C=O bonds, forming the allylic alcohols exclusively. Under the conditions for ketone hydrogenation, other reducible functional groups such as ester, lactam, and cyclopropyl ring are unaffected. The proposed mechanism involves an outer-sphere hydrogen transfer from $^{i\mathrm{Pr}}$**MnH** to the substrates followed by regeneration of the hydride through the reaction of $^{i\mathrm{Pr}}$**Mn(CO)$_2$** with H_2. Consistent with this mechanism, $^{i\mathrm{Pr}}$**MnH** catalyzes the hydrogenation of benzonitrile under similar but base-free conditions, although for some unknown reason, the addition of NaO^{t}Bu improves the catalytic efficiency. The cyclohexyl derivative $^{\mathrm{Cy}}$**MnBr** is slightly less reactive than $^{i\mathrm{Pr}}$**MnBr** in nitrile hydrogenation. Using $^{i\mathrm{Pr}}$**MnBr** and $^{\mathrm{Cy}}$**MnBr** as the precatalysts is more advantageous due to their high stability in air.

Given the availability of chiral $^{\mathrm{R}}$PN$^{\mathrm{H}}$P ligands, it is possible to develop manganese-based PNP-type catalysts for asymmetric hydrogenation of ketones. Since high temperatures often erode enantioselectivity, the reaction conditions need to be further optimized. Using phospholane-based complex **[$^{\mathrm{R*}}$Mn(CO)$_3$]$^+$** as the precatalyst and *tert*-amyl alcohol as the solvent, the Beller group was able to perform ketone hydrogenation at 40°C (Scheme 34) [58, 155]. The remarkable feature about this catalytic system is that aliphatic ketones are hydrogenated to alcohols with ee's in the 51–83% range, which is typically difficult to achieve with other catalysts. However, bulky ketones including AdCOMe, ^{t}BuCOMe, and ^{t}BuCO^{n}Pr result in low alcohol yields, and ketones of the type PhCOR′ (R′ = Me, Et, ^{n}Pr, Cy) give low ee's (11–19%). In a related study, Mezzetti explored *P*-stereogenic PNP-type manganese complexes as asymmetric hydrogenation catalysts [156]. Under the best conditions for (*S*,*S*)-[$^{\mathrm{MetBu}}$**Mn(CO)$_3$**]$^+$ (Scheme 34),

acetophenone derivatives are hydrogenated to the corresponding alcohols with ee's up to 55%. Both experimental and computational studies support the involvement of (^{R}PNP)Mn(CO)$_2$ and (^{R}PN^{H}P)Mn(CO)$_2$H in the catalytic cycle. It is interesting to know that the iron precatalyst (*S*,*S*)-**$^{Me/Bu}$FeHBr** (shown in Scheme 17) is about 30 times more active than (*S*,*S*)-**[$^{Me/Bu}$Mn(CO)$_3$]$^+$**. This is due to the formation of a more stable alkoxide species with manganese, which is generated after hydrogen transfer from (^{R}PN^{H}P)Mn(CO)$_2$H to the ketone substrate.

Esters are comparatively more challenging substrates for hydrogenation. In a 2016 report, Beller showed that at 100°C under 30 bar H_2, **^{iPr}MnBr** and **^{Cy}MnBr** (activated with KO^{t}Bu) displayed very limited catalytic activity for the hydrogenation of methyl benzoate [37]. Lan and Liu recently also reported that at 120°C under 45 bar H_2, **^{iPr}MnBr** and **^{Ph}MnBr** (activated with KO^{t}Bu) catalyzed the hydrogenation of the ketone part of methyl 4-acetylbenzoate with only 3–9% of the ester functionality being reduced [159]. However, Beller demonstrated that both **^{Et}MnBr** and **[^{Et}Mn(CO)$_3$]$^+$** were effective hydrogenation catalysts for esters, converting methyl benzoate to benzyl alcohol in 97% yield. Under the conditions outlined in Eq. 45, various aromatic and aliphatic esters including lactones can be hydrogenated to alcohols. The catalytic system shows excellent functional group compatibility, similar to the iron system described earlier (Eq. 25).

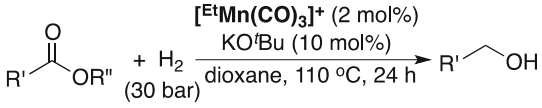

(45)

Like the ruthenium- and iron-based catalytic systems, the manganese PNP-type complexes have been tested for the hydrogenation of amides and *N*-heterocycles. Hydrogenation of PhCONHPh proved to be unsuccessful with **^{iPr}MnBr** (2 mol%, 110°C, 30 bar H_2) [159] and **[^{tBu}Mn(CO)$_2$]$^+$** (4 mol%, 130°C, 50 bar H_2) [160] in the presence of KO^{t}Bu as the activator. Catalytic hydrogenation of quinoline was shown to be feasible with the neutral dicarbonyl complexes, although the conversions were low (Eq. 46) [159]. DFT calculations suggest that the lack of activity is in part due to the low hydricity of the manganese hydride intermediate. To improve the catalysts, one of the phosphorus donor groups was replaced by a pyridine or imidazole ring, which not only increases the hydricity but also creates a less crowded environment [159, 160].

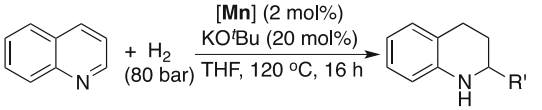

^{iPr}MnBr: 5% conversion
^{Cy}MnBr: 15% conversion
^{Ph}MnBr: 15% conversion

(46)

As suggested by DFT calculations [161], catalytic hydrogenation of CO_2 to the formate stage should be possible with the manganese-based PNP-type complexes

(e.g., ^{iPr}**Mn(CO)$_2$**), although such process has not been validated experimentally. The closest work was done by Prakash, who used ^{iPr}**MnBr** and ^{Cy}**MnBr** to catalyze the *N*-formylation of morpholine, benzylamine, and *N*-methylbenzylamine (Eq. 47) [162]. Here, the isopropyl derivative ^{iPr}**MnBr** is more efficient than ^{Cy}**MnBr**. Other amines including amylamine and *N*,*N*′-dimethylethylenediamine can also be converted to the formamides, but the yields are much lower (25–53%). The in situ generated *N*-formylmorpholine and HCONHBn can be further hydrogenated (at 150°C under 70–80 bar H_2) to methanol with TONs of up to 36, again using ^{iPr}**MnBr** as the catalyst (0.5 mol% loading). Hydrogenation of pure *N*-formylmorpholine under the same conditions gives a substantially higher TON (128) for methanol. Unfortunately, direct hydrogenation of CO_2 to methanol assisted by these amines including PEHA [89] has failed to produce any meaningful amount of methanol. This is likely due to the poisoning of the catalyst by CO_2 during the formamide hydrogenation, as described in the iron system (Scheme 20).

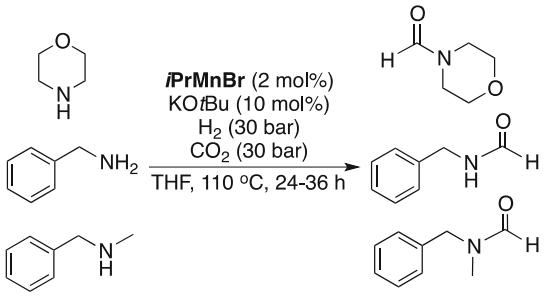

(47)

Two indirect methods of making methanol have been developed with the manganese-based PNP-type catalysts, one involving cyclic carbonates as CO_2 surrogate and the other involving CO to methanol. In 2018, Leitner demonstrated the first approach by using ^{iPr}**MnBr** as the precatalyst and NaO^{t}Bu as the activator or the in situ generated ^{iPr}**Mn(CO)$_2$** [158]. Under the best conditions for ethylene carbonate (0.1 mol% ^{iPr}**Mn(CO)$_2$**, 60 bar H_2, 120°C), ethylene glycol and methanol were obtained with TONs of 620 and 400, respectively. As shown in Eq. 48, this process can be extended to other five- and six-membered cyclic carbonates.

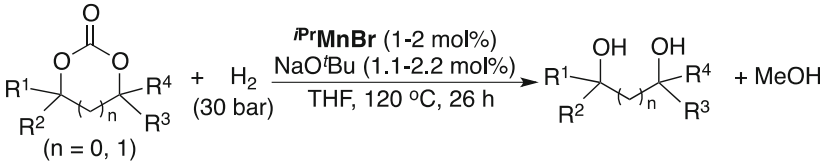

(48)

Very recently, Checinski and Beller designed a CO-to-methanol process that utilized a nitrogen-containing promoter to capture CO in the form of formamide [163]. The subsequent manganese-catalyzed formamide hydrogenation was expected to produce methanol and regenerate the promoter. After an extensive

computational screening and experimental validation, scatole and pyrrole were identified as the best promoters that balance the difficulty of amine carbonylation with that of hydrogenation to methanol. Under the optimized conditions shown in Eq. 49, methanol is obtained with high TONs. Other manganese-based PNP-type complexes have also been tested. Compared to ^{iPr}**MnBr**, ^{Cy}**MnBr**, ^{Et}**MnBr**, and **[^{Et}Mn(CO)$_3$]$^+$** are slightly less active, whereas ^{Ph}**MnBr** and **[^{tBu}Mn(CO)$_2$]$^+$** are almost inactive. The methylated complex (^{Et}PN^{Me}P)Mn(CO)$_2$Br also displays limited reactivity, suggesting that in this case, the presence of the NH moiety is critical to the success of the hydrogenation process.

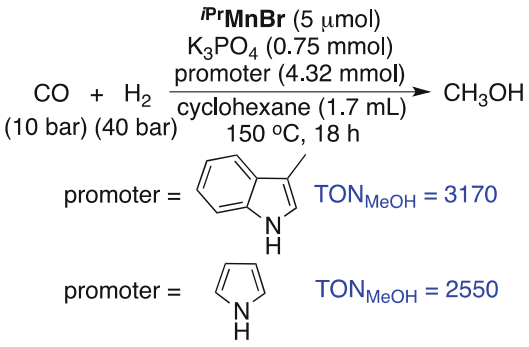

(49)

7.2 *Rhenium Catalysts*

Rhenium-based PNP-type complexes have been prepared following the procedures established for the manganese system. The reaction of ^{iPr}PN^{H}P with ReBr(CO)$_5$ produces **[^{iPr}Re(CO)$_3$]$^+$** in which the PNP ligand adopts the facial coordination mode (Eq. 50) [164]. In contrast, the phospholane-based PNP ligand coordinates to the Re(CO)$_3^+$ fragment in a meridional fashion [58].

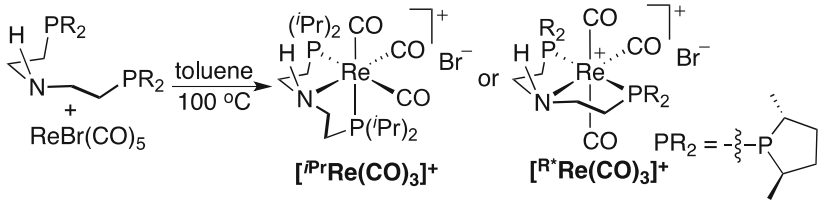

(50)

Both **[^{iPr}Re(CO)$_3$]$^+$** and **[^{R*}Re(CO)$_3$]$^+$** have been employed to catalyze the hydrogenation of ketones. Under the optimized conditions for **[^{iPr}Re(CO)$_3$]$^+$** (Scheme 35), most functional groups are tolerated with cyano, phenol, and boric acid being the exceptions [164]. While isolated C=C bonds and internal C ≡ C

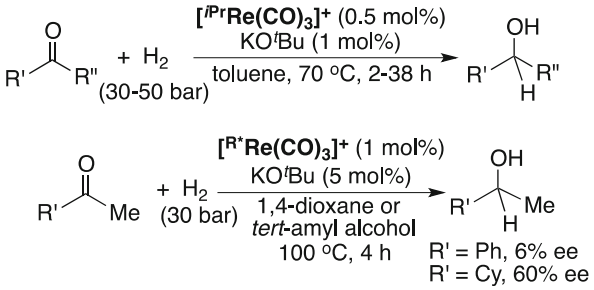

Scheme 35 Rhenium-catalyzed hydrogenation of ketones

bonds are intact during the hydrogenation, α,β-unsaturated ketones typically give saturated alcohols as the major or sole products. Hydrogenation of $R'COCH_2CH_2CO_2Me$ provides γ-butyrolactones, although a higher loading of $[^{iPr}Re(CO)_3]^+$ (5 mol%) and KO^{t}Bu (10 mol%) is needed. Using the chiral precatalyst $[^{R*}Re(CO)_3]^+$ results in low ee for hydrogenating acetophenone and moderate ee for hydrogenating cyclohexyl methyl ketone [58]. This level of enantioselectivity is lower than that achieved with the manganese analog but comparable to the ruthenium- and iron-based catalytic systems.

8 Summary and Outlook

The use of the $^{R}PN^{H}P$ ligands to design hydrogenation catalysts has been a fruitful patch in the field of homogeneous catalysis. As shown in this chapter, transition metal complexes supported by these ligands along with strong-field ligands such as CO, NO, and isocyanides have been so extensively studied that most of the mid- and late-transition metals have been involved. Some of the hydrogenation processes do not require the NH moiety. Examples include hydrogenation of weakly polarized C=C bonds and hydrogenation of CO_2 to formate. However, metal-ligand cooperativity enabled by the NH functionality does have advantage for the more challenging hydrogenation processes such as CO_2 hydrogenation to methanol and amide hydrogenation.

We envision that interests in using $^{R}PN^{H}P$ ligated complexes for catalytic hydrogenation reactions will continue to grow in the future. In particular, group 5 and group 11 metals have not been explored to build PNP-type complexes specifically for hydrogenation reactions. A recent computation study focusing on ($^{iPr}PN^{H}P$)M$(NO)_2H$ (M = V, Nb, Ta; see Fig. 6) suggests that they are promising catalysts [165]. Inspired by the structure of the active site of [Fe]-hydrogenase, Yang has computationally designed PNP-type complexes of iron [166] and cobalt [167] that contain acylmethylpyridinol as the ancillary ligand. These molecules present significant synthetic challenges but may provide a path for synthetic chemists to identify more robust and active hydrogenation catalysts.

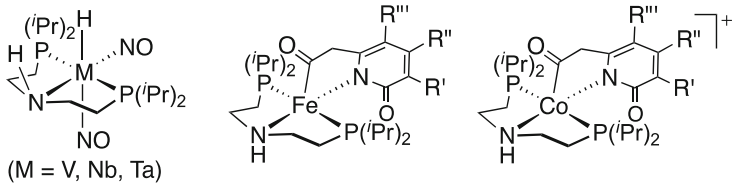

Fig. 6 Computationally designed hydrogenation catalysts

References

1. de Vries JG, Elsevier CJ (eds) (2007) The handbook of homogeneous hydrogenation. Wiley-VCH, Weinheim
2. Clarke ML (2012) Cat Sci Technol 2:2418
3. Werkmeister S, Junge K, Beller M (2014) Org Process Res Dev 18:289
4. Alig L, Fritz M, Schneider S (2019) Chem Rev 119:2681
5. Osborn JA, Jardine FH, Young JF, Wilkinson G (1966) J Chem Soc A:1711
6. Halpern J (1982) Science 217:401
7. Hallman PS, McGarvey BR, Wilkinson G (1968) J Chem Soc A:3143
8. Noyori R, Ohkuma T (2001) Angew Chem Int Ed 40:40
9. Shambayati S, Crowe WE, Schreiber SL (1990) Angew Chem Int Ed Engl 29:256
10. Zhang J, Leitus G, Ben-David Y, Milstein D (2006) Angew Chem Int Ed 45:1113
11. Saudan LA, Saudan CM, Debieux C, Wyss P (2007) Angew Chem Int Ed 46:7473
12. Ito M, Koo LW, Himizu A, Kobayashi C, Sakaguchi A, Ikariya T (2009) Angew Chem Int Ed 48:1324
13. Balaraman E, Gnanaprakasam B, Shimon LJW, Milstein D (2010) J Am Chem Soc 132:16756
14. Casey CP, Guan H (2007) J Am Chem Soc 129:5816
15. Sui-Seng C, Freutel F, Lough AJ, Morris RH (2008) Angew Chem Int Ed 47:940
16. Zhang G, Scott BL, Hanson SK (2012) Angew Chem Int Ed 51:12102
17. Shvo Y, Czarkie D, Rahamim Y, Chodosh DF (1986) J Am Chem Soc 108:7400
18. Ohkuma T, Ooka H, Hashiguchi S, Ikariya T, Noyori R (1995) J Am Chem Soc 117:2675
19. Doucet H, Ohkuma T, Murata K, Yokozawa T, Kozawa M, Katayama E, England AF, Ikariya T, Noyori R (1998) Angew Chem Int Ed 37:1703
20. Sui-Seng C, Haque FN, Hadzovic A, Pütz A-M, Reuss V, Meyer N, Lough AJ, Zimmer-De Iuliis M, Morris RH (2009) Inorg Chem 48:735
21. Otsuka T, Ishii A, Dub PA, Ikariya T (2013) J Am Chem Soc 135:9600
22. Qu S, Dai H, Dang Y, Song C, Wang Z-X, Guan H (2014) ACS Catal 4:4377
23. Sandoval CA, Ohkuma T, Muñiz K, Noyori R (2003) J Am Chem Soc 125:13490
24. Werkmeister S, Junge K, Wendt B, Alberico E, Jiao H, Baumann W, Junge H, Gallou F, Beller M (2014) Angew Chem Int Ed 53:8722
25. Dub PA, Gordon JC (2017) ACS Catal 7:6635
26. Smith NE, Bernskoetter WH, Hazari N (2019) J Am Chem Soc 141:17350
27. Dub PA, Gordon JC (2018) Nat Rev Chem 2:396
28. Dub PA, Scott BL, Gordon JC (2017) J Am Chem Soc 139:1245
29. Werkmeister S, Neumann J, Junge K, Beller M (2015) Chem Eur J 21:12226
30. Wilson ME, Nuzzo RG, Whitesides GM (1978) J Am Chem Soc 100:2269
31. Hermosilla P, López P, García-Orduña P, Lahoz FJ, Polo V, Casado MA (2018) Organometallics 37:2618
32. Kuriyama W, Matsumoto T, Ino Y, Ogata O (2011) PCT Int Appl WO/2011/048727 A1
33. Danopoulos AA, Wills AR, Edwards PG (1990) Polyhedron 9:2413

34. Ma W, Cui S, Sun H, Tang W, Xue D, Li C, Fan J, Xiao J, Wang C (2018) Chem Eur J 14:13118
35. Abdur-Rashid K, Graham T, Tsang C-W, Chen X, Guo R, Jia W, Amoroso D, Sui-Seng C (2008) PCT Int Appl WO/2008/141439 A1
36. Meiners J, Friedrich A, Herdtweck E, Schneider S (2009) Organometallics 28:6331
37. Elangovan S, Garbe M, Jiao H, Spannenberg A, Junge K, Beller M (2016) Angew Chem Int Ed 55:15364
38. Burk MJ, Feaster JE, Harlow RL (1991) Tetrahedron Asymmetry 2:569
39. Huber R, Passera A, Gubler E, Mezzetti A (2018) Adv Synth Catal 360:2900
40. Schneider S, Meiners J, Askevold B (2012) Eur J Inorg Chem:412
41. Coles SJ, Edwards PG, Hursthouse MB, Read PW (1994) J Chem Soc Chem Commun:1967
42. Coles SJ, Danopoulos AA, Edwards PG, Hursthouse MB, Read PW (1995) J Chem Soc Dalton Trans:3401
43. Sherwood R, Gonzàlez de Rivera F, Wan JH, Zhang Q, White AJP, Rossell O, Hogarth G, Wilton-Ely JDET (2015) Inorg Chem 54:4222
44. García-Seijo MI, Habtemariam A, Parsons S, Gould RO, García-Fernández ME (2002) New J Chem 26:636
45. Fillman KL, Bielinski EA, Schmeier TJ, Nesvet JC, Woodruff TM, Pan CJ, Takase MK, Hazari N, Neidig ML (2014) Inorg Chem 53:6066
46. Ma W, Cui S, Sun H, Tang W, Xue D, Li C, Fan J, Xiao J, Wang C (2018) Chem Eur J 24:13118
47. Nguyen DH, Morin Y, Zhang L, Trivelli X, Capet F, Paul S, Desset S, Dumeignil F, Gauvin RM (2017) ChemCatChem 9:2652
48. Junge K, Wendt B, Cingolani A, Spannenberg A, Wei Z, Jiao H, Beller M (2018) Chem Eur J 24:1046
49. Rozenel SS, Kerr JB, Arnold J (2011) Dalton Trans 40:10397
50. Shao Z, Fu S, Wei M, Zhou S, Liu Q (2016) Angew Chem Int Ed 55:14653
51. Lagaditis PO, Schluschaß B, Demeshko S, Würtele C, Schneider S (2016) Inorg Chem 55:4529
52. Fu S, Chen N-Y, Liu X, Shao Z, Luo S-P, Liu Q (2016) J Am Chem Soc 138:8588
53. Zhou W, Wei Z, Spannenberg A, Jiao H, Junge K, Jung H, Beller M (2019) Chem Eur J 25:8459
54. Kuriyama W, Matsumoto T, Ogata O, Ino Y, Aoki K, Tanaka S, Ishida K, Kobayashi T, Sayo N, Saito T (2012) Org Process Res Dev 16:166
55. Han Z, Rong L, Wu J, Zhang L, Wang Z, Ding K (2012) Angew Chem Int Ed 51:13041
56. Zhang L, Raffa G, Nguyen DH, Swesi Y, Corbel-Demailly L, Capet F, Trivelli X, Desset S, Paul S, Paul J-F, Fongarland P, Dumeignil F, Gauvin RM (2016) J Catal 340:331
57. Bertoli M, Choualeb A, Lough AJ, Moore B, Spasyuk D, Gusev DG (2011) Organometallics 30:3479
58. Garbe M, Wei Z, Tannert B, Spannenberg A, Jiao H, Bachmann S, Scalone M, Junge K, Beller M (2019) Adv Synth Catal 361:1913
59. Touge T, Aoki K, Nara H, Kuriyama W (2012) PCT Int Appl WO/2012/144650 A1
60. Nielsen M, Alberico E, Baumann W, Drexler H-J, Junge H, Gladiali S, Beller M (2013) Nature 495:85
61. Choi J-H, Schloerer NE, Berger J, Prechtl MHG (2014) Dalton Trans 43:290
62. Choi J-H, Heim LE, Ahrens M, Prechtl MHG (2014) Dalton Trans 43:17248
63. Ogata O, Nakayama Y, Nara H, Fujiwhara M, Kayaki Y (2016) Org Lett 18:3894
64. Lazzari D, Cassani MC, Bertola M, Casado Moreno F, Torrente D (2013) RSC Adv 3:15582
65. Deutsch J, Jiménez Pinto J, Doerfelt S, Martin A, Köckritz A (2015) Flavour Fragr J 30:101
66. Fairweather NT, Gibson MS, Guan H (2015) Organometallics 34:335
67. Nguyen DH, Raffa G, Morin Y, Desset S, Capet F, Nardello-Rataj V, Dumeignil F, Gauvin RM (2017) Green Chem 19:5665
68. Ziebart C, Jackstell R, Beller M (2013) ChemCatChem 5:3228

69. Satapathy A, Gadge ST, Bhanage BM (2017) ChemSusChem 10:1356
70. Gao S, Tang W, Zhang M, Wang C, Xiao J (2016) Synlett:1748
71. Padilla R, JØrgensen MSB, Paixão MW, Nielsen M (2019) Green Chem 21:5195
72. Pittaway R, Fuentes JA, Clarke ML (2017) Org Lett 19:2845
73. Chen J, Wang J, Tu T (2018) Chem Asian J 13:2559
74. Thiyagarajan S, Gunanathan C (2019) Org Lett 21:9774
75. Neumann J, Bornschein C, Jiao H, Junge K, Beller M (2015) Eur J Org Chem:5944
76. Choi J-H, Prechtl MHG (2015) ChemCatChem 7:1023
77. Wei Q, Zhang F, Zhao X, Wang C, Xiao J, Tang W (2017) Org Biomol Chem 15:5468
78. Wang W-H, Himeda Y, Muckerman JT, Manbeck GF, Fujita E (2015) Chem Rev 115:12936
79. Liu Q, Wu L, Gülak S, Rockstroh N, Jackstell R, Beller M (2014) Angew Chem Int Ed 53:7085
80. Treigerman Z, Sasson Y (2018) ACS Omega 3:12797
81. Kothandaraman J, Czaun M, Goeppert A, Haiges R, Jones J-P, May RB, Prakash GKS, Olah GA (2015) ChemSusChem 8:1442
82. Zhang L, Han Z, Zhao X, Wang Z, Ding K (2015) Angew Chem Int Ed 54:6186
83. Koo J, Kim SH, Hong SH (2018) Chem Commun 54:4995
84. Kar S, Goeppert A, Prakash GKS (2019) J Am Chem Soc 141:12518
85. Dong K, Elangovan S, Sang R, Spannenberg A, Jackstell R, Junge K, Li Y, Beller M (2016) Nat Commun 7:12075
86. Rezayee NM, Huff CA, Sanford MS (2015) J Am Chem Soc 137:1028
87. Kothandaraman J, Goeppert A, Czaun M, Olah GA, Prakash GKS (2016) J Am Chem Soc 138:778
88. Kothandaraman J, Goeppert A, Czaun M, Olah GA, Prakash GKS (2016) Green Chem 18:5831
89. Kar S, Sen R, Goeppert A, Prakash GKS (2018) J Am Chem Soc 140:1580
90. Yoshimura A, Watari R, Kuwata S, Kayaki Y (2019) Eur J Inorg Chem:2375
91. Kothandaraman J, Kar S, Sen R, Goeppert A, Olah GA, Prakash GKS (2017) J Am Chem Soc 139:2549
92. Kar S, Sen R, Kothandaraman J, Goeppert A, Chowdhury R, Munoz SB, Haiges R, Prakash GKS (2019) J Am Chem Soc 141:3160
93. Schneck F, Assmann M, Balmer M, Harms K, Langer R (2016) Organometallics 35:1931
94. Alberico E, Sponholz P, Cordes C, Nielsen M, Drexler H-J, Baumann W, Junge H, Beller M (2013) Angew Chem Int Ed 52:14162
95. Chakraborty S, Dai H, Bhattacharya P, Fairweather NT, Gibson MS, Krause JA, Guan H (2014) J Am Chem Soc 136:7869
96. Elangovan S, Wendt B, Topf C, Bachmann S, Scalone M, Spannenberg A, Jiao H, Baumann W, Junge K, Beller M (2016) Adv Synth Catal 358:820
97. Rezayee NM, Samblanet DC, Sanford MS (2016) ACS Catal 6:6377
98. Lange S, Elangovan S, Cordes C, Spannenberg A, Jiao H, Junge H, Bachmann S, Scalone M, Topf C, Junge K, Beller M (2016) Cat Sci Technol 6:4768
99. Koehne I, Schmeier TJ, Bielinski EA, Pan CJ, Lagaditis PO, Bernskoetter WH, Takase MK, Würtele C, Hazari N, Schneider S (2014) Inorg Chem 53:2133
100. Chakraborty S, Brennessel WW, Jones WD (2014) J Am Chem Soc 136:8564
101. Bielinski EA, Lagaditis PO, Zhang Y, Mercado BQ, Würtele C, Bernskoetter WH, Hazari N, Schneider S (2014) J Am Chem Soc 136:10234
102. Smith NE, Bernskoetter WH, Hazari N, Mercado BQ (2017) Organometallics 36:3995
103. Yi Y, Liu H, Xiao L-P, Wang B, Song G (2018) ChemSusChem 11:1474
104. Bonitatibus Jr PJ, Chakraborty S, Doherty MD, Siclovan O, Jones WD, Soloveichik GL (2015) Proc Natl Acad Sci U S A 112:1687
105. Chakraborty S, Lagaditis PO, Förster M, Bielinski EA, Hazari N, Holthausen MC, Jones WD, Schneider S (2014) ACS Catal 4:3994

106. Lagaditis PO, Sues PE, Sonnenberg JF, Wan KY, Lough AJ, Morris RH (2014) J Am Chem Soc 136:1367
107. Sonnenberg JF, Lagaditis PO, Lough AJ, Morris RH (2014) Organometallics 33:6452
108. Smith SAM, Lagaditis PO, Lüpke A, Lough AJ, Morris RH (2017) Chem Eur J 23:7212
109. Seo CSG, Tannoux T, Smith SAM, Lough AJ, Morris RH (2019) J Org Chem 84:12040
110. Jayarathne U, Zhang Y, Hazari N, Bernskoetter WH (2017) Organometallics 36:409
111. Bornschein C, Werkmeister S, Wendt B, Jiao H, Alberico E, Baumann W, Junge H, Junge K, Beller M (2014) Nat Commun 5:4111
112. Sawatlon B, Surawatanawong P (2016) Dalton Trans 45:14965
113. Xu R, Chakraborty S, Bellows SM, Yuan H, Cundari TR, Jones WD (2016) ACS Catal 6:2127
114. Bernskoetter WH, Hazari N (2017) Acc Chem Res 50:1049
115. Zhang Y, MacIntosh AD, Wong JL, Bielinski EA, Williard PG, Mercado BQ, Hazari N, Bernskoetter WH (2015) Chem Sci 6:4291
116. Curley JB, Smith NE, Bernskoetter WH, Hazari N, Mercado BQ (2018) Organometallics 37:3846
117. Jayarathne U, Hazari N, Bernskoetter WH (2018) ACS Catal 8:1338
118. Suàrez LA, Culakova Z, Balcells D, Bernskoetter WH, Eisenstein O, Goldberg KI, Hazari N, Tilset M, Nova A (2018) ACS Catal 8:8751
119. Lane EM, Zhang Y, Hazari N, Bernskoetter WH (2019) Organometallics 38:3084
120. Jiao H, Junge K, Alberico E, Beller M (2016) J Comput Chem 37:168
121. Acosta-Ramirez A, Bertoli M, Gusev DG, Schlaf M (2012) Green Chem 14:1178
122. Taqui Khan MM, Khan BT, Begum S, Nazeeruddin K (1984) J Mol Catal 26:207
123. Taqui Khan MM, Khan BT, Begum S, Ali SM (1986) J Mol Catal 34:283
124. Taqui Khan MM, Khan BT, Begum S (1987) React Kinet Catal Lett 34:105
125. Taqui Khan MM, Khan BT, Begum S (1986) J Mol Catal 34:9
126. Taqui Khan MM, Rao ER, Siddiqui MRH, Khan BT, Begum S, Ali SM, Reddy J (1988) J Mol Catal 45:35
127. Ramaraj A, Nethaji M, Jagirdar BR (2019) J Organomet Chem 883:25
128. Rozenel SS, Padilla R, Camp C, Arnold J (2014) Chem Commun 50:2612
129. Zhang G, Vasudevan KV, Scott BL, Hanson SK (2013) J Am Chem Soc 135:8668
130. Mills MR, Barnes CL, Bernskoetter WH (2018) Inorg Chem 57:1590
131. Jing Y, Chen X, Yang X (2015) Organometallics 34:5716
132. Yuwen J, Chakraborty S, Brennessel WW, Jones WD (2017) ACS Catal 7:3735
133. Chowdhury A, Biswas S, Pramanik A, Sakar P (2019) Dalton Trans 48:16083
134. Dai H, Guan H (2018) ACS Catal 8:9125
135. Schneekönig J, Tannert B, Hornke H, Beller M, Junge K (2019) Cat Sci Technol 9:1779
136. Xu S, Chakraborty S, Yuan H, Jones WD (2015) ACS Catal 5:6350
137. Spentzos AZ, Barnes CL, Bernskoetter WH (2016) Inorg Chem 55:8225
138. Clarke ZE, Maragh PT, Dasgupta TP, Gusev DG, Lough AJ, Abdur-Rashid K (2006) Organometallics 25:4113
139. Chen X, Jia W, Guo R, Graham TW, Gullons MA, Abdur-Rashid K (2009) Dalton Trans:1407
140. Junge K, Wendt B, Jiao H, Beller M (2014) ChemCatChem 6:2810
141. Schmeier TJ, Dobereiner GE, Crabtree RH, Hazari N (2011) J Am Chem Soc 133:9274
142. Vasudevan KV, Scott BL, Hanson SK (2012) Eur J Inorg Chem:4898
143. Taqui Khan MM, Khan BT, Begum S (1988) J Mol Catal 45:305
144. McGuinness DS, Brown DB, Tooze RP, Hess FM, Dixon JT, Slawin AMZ (2006) Organometallics 25:3605
145. McGuinness DS, Wassercheid P, Keim W, Hu C, Englert U, Dixon JT, Grove C (2003) Chem Commun:334
146. Chakraborty S, Blacque O, Fox T, Berke H (2014) Chem Asian J 9:328
147. Chakraborty S, Berke H (2014) ACS Catal 4:2191
148. Wei Z, Junge K, Beller M, Jiao H (2017) Cat Sci Technol 7:2298
149. Chakraborty S, Blacque O, Berke H (2015) Dalton Trans 44:6560

150. Leischner T, Spannenberg A, Junge K, Beller M (2018) Organometallics 37:4402
151. Leischner T, Suarez LA, Spannenberg A, Junge K, Nova A, Beller M (2019) Chem Sci 10:10566
152. Zell T, Langer R (2018) ChemCatChem 10:1930
153. Elangovan S, Topf C, Fischer S, Jiao H, Spannenberg A, Baumann W, Ludwig R, Junge K, Beller M (2016) J Am Chem Soc 138:8809
154. Fu S, Shao Z, Wang Y, Liu Q (2017) J Am Chem Soc 139:11941
155. Garbe M, Junge K, Walker S, Wei Z, Jiao H, Spannenberg A, Bachmann S, Scalone M, Beller M (2017) Angew Chem Int Ed 56:11237
156. Passera A, Mezzetti A (2019) Adv Synth Catal 361:4691
157. Jang YK, Krückel T, Rueping M, El-Sepelgy O (2018) Org Lett 20:7779
158. Kaithal A, Hölscher M, Leitner W (2018) Angew Chem Int Ed 57:13449
159. Wang Y, Zhu L, Shao Z, Li G, Lan Y, Liu Q (2019) J Am Chem Soc 141:17337
160. Papa V, Carbero-Antonino JR, Alberico E, Spannenberg A, Junge K, Junge H, Beller M (2017) Chem Sci 8:3576
161. Rawat KS, Pathak B (2017) Cat Sci Technol 7:3234
162. Kar S, Goeppert A, Kothandaraman J, Prakash GKS (2017) ACS Catal 7:6347
163. Ryabchuk P, Stier K, Junge K, Checinski MP, Beller M (2019) J Am Chem Soc 141:16923
164. Wei D, Roisnel T, Darcel C, Clot E, Sortais J-B (2017) ChemCatChem 9:80
165. Wei Z, Junge K, Beller M, Jiao H (2018) CR Chim 21:303
166. Yang X (2015) Chem Commun 51:13098
167. Ge H, Jing Y, Yang X (2016) Inorg Chem 55:12179